water

MDPI

Article

Sediment Balance Estimation of the 'Cuvette Centrale' of the Congo River Basin Using the SWAT Hydrological Model

Pankyes Datok [1,*], Sabine Sauvage [1,*], Clément Fabre [2], Alain Laraque [3], Sylvain Ouillon [4,5], Guy Moukandi N'kaya [6] and José-Miguel Sanchez-Perez [1]

1 Laboratoire Ecologie Fonctionnelle et Environnement, Université de Toulouse, CNRS, INPT, UPS, 31326 Toulouse, France; jose-miguel.sanchez-perez@univ-tlse3.fr
2 Eawag, Swiss Federal Institute of Aquatic Science and Technology, CH-8600 Dübendorf, Switzerland; clement.fabre21@gmail.com
3 GET, UMR CNRS/IRD/UPS, 31400 Toulouse, France; alain.laraque@ird.fr
4 LEGOS, Université de Toulouse, IRD, CNRS, CNES, UPS, 31400 Toulouse, France; sylvain.ouillon@legos.obs-mip.fr
5 USTH, Vietnam Academy of Science and Technology (VAST), Hanoi 100000, Vietnam
6 LMEI/CUSI/ENSP/Université Marien Ngouabi, Brazzaville BP 69, Congo; guymoukandi@yahoo.fr
* Correspondence: pankyes-emmanuel.datok@univ-tlse3.fr (P.D.); sabine.sauvage@univ-tlse3.fr (S.S.)

Abstract: In this study, the SWAT hydrological model was used to estimate the sediment yields in the principal drainage basins of the Congo River Basin. The model was run for the 2000–2012 period and calibrated using measured values obtained at the basins principal gauging station that controls 98% of the basin area. Sediment yield rates of 4.01, 5.91, 7.88 and 8.68 t km^{-2} yr^{-1} were estimated for the areas upstream of the Ubangi at Bangui, Sangha at Ouesso, Lualaba at Kisangani, and Kasai at Kuto-Moke, respectively—the first three of which supply the Cuvette Centrale. The loads contributed into the Cuvette Centrale by eight tributaries were estimated to be worth 0.04, 0.07, 0.09, 0.18, 0.94, 1.50, 1.60, and 26.98 × 10^6 t yr^{-1} from the Likouala Mossaka at Makoua, Likouala aux Herbes at Botouali, Kouyou at Linnegue, Alima at Tchikapika, Sangha at Ouesso, Ubangi at Mongoumba, Ruki at Bokuma and Congo at Mbandaka, respectively. The upper Congo supplies up to 85% of the fluxes in the Cuvette Centrale, with the Ubangi and the Ruki contributing approximately 5% each. The Cuvette Centrale acts like a big sink trapping up to 23 megatons of sediment produced upstream (75%) annually.

Keywords: Congo River Basin; Cuvette Centrale; erosion; sediment transport; sediment balance; SWAT

Citation: Datok, P.; Sauvage, S.; Fabre, C.; Laraque, A.; Ouillon, S.; Moukandi N'kaya, G.; Sanchez-Perez, J.-M. Sediment Balance Estimation of the 'Cuvette Centrale' of the Congo River Basin Using the SWAT Hydrological Model. *Water* **2021**, *13*, 1388. https://doi.org/10.3390/w13101388

Academic Editor: Bommanna Krishnappan

Received: 20 April 2021
Accepted: 14 May 2021
Published: 16 May 2021

1. Introduction

The most important agent transporting sediment across the land is river transport, while relief and runoff are the most important factors determining the sediment load of rivers [1] (Hay, 1998). The suspended sediment load transported by a river or stream is a mixture of sediment derived from different areas in a catchment that comprise source types with different erosional processes depending on the time and place [2,3] (Walling, 2006; Haddadchi et al., 2013). Sediment fluxes and their variability are important and merit study because drastic changes in their amounts and patterns usually indicate additional human impacts on the basin [4,5] (NKounkou & Probst, 1987; Walling, 2009).

Wetlands are complex ecosystems that act as an interface between terrestrial and aquatic ecosystems. Wetlands receive water and sediments from external sources [6] (Mitsch & Gooselink, 2015). The hydrodynamic characteristics of wetland ecosystems, including the water inputs, outputs, water flow, and seasonality, can influence organic deposition and material fluxes [7] (Gosselink & Turner, 1978). [8] Novitzki (1979) characterized wetlands with regard to water source and landform as surface or groundwater depressions or slopes, which are defined by whether or not they receive a greater amount

of water from precipitation and overland flow or by their intersection of the water table. Therefore, the type of wetland will play a significant role in the sediment dynamics of a catchment, as one of the specific functions of wetlands is serving as a sediment trap [6,9,10] (Laraque et al., 2009; Mitsch & Gooselink, 2015; Mitsch et al., 2015).

The Congo River Basin (CRB) is the second-largest continuous tropical rainforest in the world and hosts the largest peatland complex found anywhere in Africa [11] (Dargie et al., 2017). Peatlands are the largest natural terrestrial carbon store, helping to minimise flood and drought risk, retaining sediment and preserving global biodiversity [12] (Harenda et al., 2018). The central depression in the heart of this basin, famously called the "Cuvette Centrale", encircles the peatland complex. There are important spatial variations in the tributaries that supply the Cuvette Centrale with water, sediments and nutrients. These tributaries are located both on the right bank and on the left bank tributaries of the main Congo River. These variations are due to the position of the basin straddling the equator, which results in different precipitation patterns on both sides of the hemisphere. A few authors have studied the material fluxes of the Congo basin [9,13–20] (Probst, 1983; Probst et al., 1992; Moukolo et al., 1993; Gaillardet et al., 1995; Dupré et al., 1996; Guyot et al., 2000; Seyler et al., 2006; Laraque et al., 2009; Mushi et al., 2019). These studies have quantified fluxes as part of a global study or estimated material fluxes at the outlets of major tributaries using hydro-sedimentary budgets based on in situ data, models or remote sensing methods. While they have laid appreciable foundations for further study, there remains a lot to be understood given the new information and dynamics regarding peatland stock and the changing precipitation patterns over some major tributaries occasioned by climate change [11,21,22] (Gumbricht et al., 2017; Dargie et al., 2017; Nguimalet & Orange, 2019).

The importance of the Cuvette Centrale cannot be over-emphasized. Given its role as a globally important asset in the fight against climate change, biodiversity loss, and social instability in the region. An analysis of the nature of wetland material, their particulate and dissolved fluxes, spatial and temporal variability could provide important indicators of climatic and environmental change and anthropogenic factors causing these changes. The sources of "Cuvette Centrale" sediment-laden waters, whether through smaller or larger streams, as well as the dynamics of the loads they carry, remains a grey area. In addition, erosional processes have not been clearly understood, while the spatio-temporal variations in sediment dynamics within the basin have more questions than answers [17] (Mushi et al., 2019). Several factors are responsible for the fluvial transport of sediments to the ocean. It is important to study them to better assess their effect on the environment at whatever scale [5,23] (Walling, 2009; Aagaard & Hughes, 2013). In addition to identifying potential sediment source areas, it is useful to estimate the volumes of sediment that are carried into the reach, as declining or increased sediment supply can influence wetland stability [24,25] (Oeurng et al., 2011; Guan et al., 2017).

This paper uses modelling tools to estimate sediment yields in the sub-basins and fluxes transported in the important tributaries of the Congo basin. While other studies have conducted independent assessments of the yields in specific sub-basins, we have considered the tributaries that feed into the Cuvette Centrale from both northern and southern tributaries taking note of the spatio-temporal variations in these tributaries. Specifically, this study aims to: (i) quantify the sediment fluxes in the CRB based on daily discharge and suspended sediment concentration; (ii) identify the important contributing tributaries as well as the critical source areas and (iii) estimate, for the first time, an upstream-downstream sediment balance within the Central Cuvette. This study is carried out for the 2000 to 2012 period, assuming that this period represents the hydro-sedimentary chronicle of the Congo basin [26–28] (Laraque et al., 2020; Moukandi N'kaya et al., 2020, 2021). It is also important to note that this study considers only the suspended sediments without the bedload component. The study also discusses the role played by the Cuvette Centrale in the hydro-sedimentary budget of the Congo basin.

2. Materials and Methods

2.1. Study Area

2.1.1. General Characteristics

The CRB is the second largest river basin and the second largest area of contiguous tropical rainforest in the world. In Africa, it drains ten countries [29] (BRLi, 2016), partly or wholly, located both on the northern and southern hemispheres (Figure 1). At the Brazzaville/Kinshasa-gauging station, its size corresponds to 3.7 million km^2 and its mean discharge measured from 1902 to 2011 is 41,100 m^3 s^{-1} [29] (BRLi, 2016). The Congo basin is an intra-continental sedimentary basin encircled by relatively gentle relief (except for a few volcanoes on its eastern border, see Figure 2c), drained by numerous tributaries of the main Congo River [30] (Kadima et al., 2011). Its internal broad bowl-shaped sedimentary depression or "sag basin", generally referred to as the Cuvette Centrale [30–33] (Daly et al., 1992; Laraque et al., 1998b; Kadima et al. 2011; Alsdorf et al., 2016), results from the geodynamic influence of tectonic events [30] (Kadima et al. 2011). Its size is 1.2 million km^2 between 3°S-1°N latitude and 18–22° E longitude [31] (Daly et al., 1992), 32% (360,000 km^2) of which corresponds to wetlands [34] (Bwangoy et al., 2010).

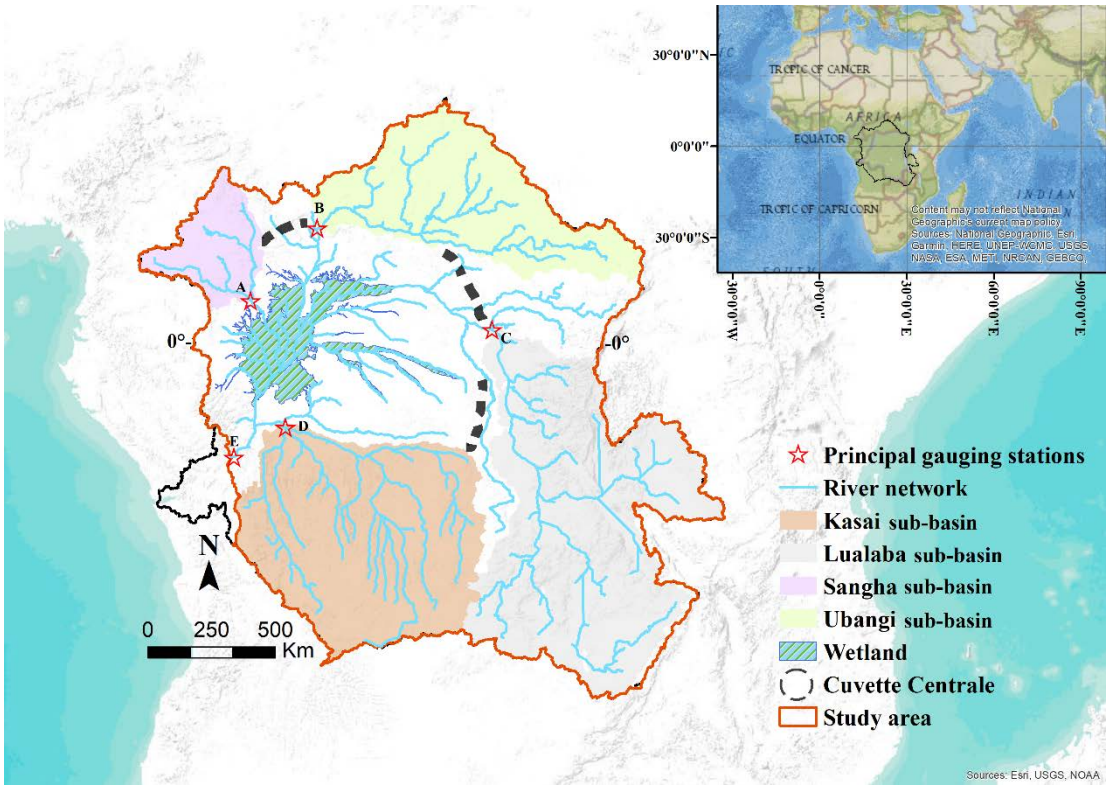

Figure 1. Map of the Congo basin showing its location in Africa, river network above the main gauging station of the Congo River at Brazzaville/Kinshasa (E), the principal gauging stations of Sangha at Ouesso (A), Ubangi at Bangui (B), Lualaba at Kisangani (C), and Kasai at Kutu Moke (D). The extent of the Cuvette Centrale (sensu lato) is also shown [26] (after Laraque et al., 2020), and the wetlands of the Cuvette Centrale were extracted from the global wetland database [35] (Lehner & Doll, 2004).

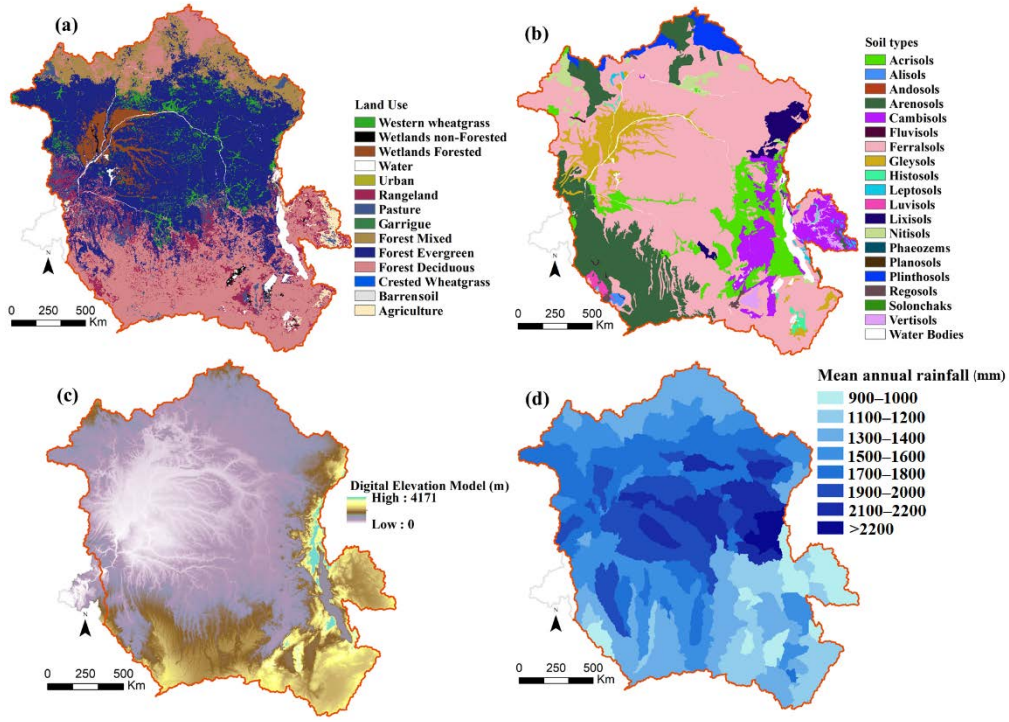

Figure 2. Maps of (**a**) land use (Global Land Cover 2000 database); (**b**) soils (Harmonized World Soil Database v 1.1); (**c**) Digital Elevation Model (Consortium for spatial information); and (**d**) simulated precipitation from the TRMM product (Multi-satellite precipitation analysis) used as inputs in the SWAT model. The map references and resolutions are listed in Table 1.

The main drainage systems of the basin are the Ubangi and Sangha catchments in the north and the Lualaba and Kasai catchments in the south, which are separated by the equator (Figure 1). Their tributaries converge and join the Congo main stem in the middle of the basin. Precipitation and hydrological regimes over the basin are bimodal and typical of equatorial regions, with the main flood from November to January and a lesser flood from April to June [28] (Moukandi et al., 2021). Annual average rainfall in the Cuvette Central are over 2000 mm yr^{-1} and decrease to as low as 1000 mm yr^{-1} in the northern and southern portions of the basin ([33] Alsdorf et al., 2016, see Figure 2d). The Cuvette Centrale is estimated to accumulate up to 9 km of sediment over much of geological time [36] (Crosby et al., 2010). The lithology of the basin comprises chiefly of alluvium, metamorphic and clastic sediments with most of the groundwater stored in permeable unconsolidated alluvium that could reach 400 m deep [37,38] (UNESCO, 2004; Schlueter, 2006). Dominant soil classes in the basin are ferralsols, arenosols, and nitisols (Figure 2b). Sands and clays dominate the basin soils with clay proportions dominating the Cuvette Centrale and the Sangha basin while sands dominate in the southern parts of the basin [17,39] (Mushie et al., 2019; Kabuya et al., 2020). The land cover of the basin consists of evergreen forests in the central basin with other uses such as agriculture, pasture and water bodies (Figure 2a).

2.1.2. Hydro-Sedimentary Measurements in the Congo River Basin

The Congo River Basin (CRB) is among the least studied river basins in the world [26,33] (Alsdorf et al., 2016; Laraque et al., 2020). Hydro-pluviometric networks have existed in the basin since colonial times. Some of the first analyses of material, both solid and dissolved, were carried out at the Brazzaville/Kinshasa gauge station in the early part of the 20th century. Discharge measurements have existed mainly at the Brazzaville/Kinshasa station, which controls 98% of the CRB. Monthly measurements of selected biogeochemical parameters have been carried out during the 1987–1994 period and continuously since 2005 until date. [26] Laraque et al. (2020) gives a chronological summary of the measure-

ments of concentrations of Total Suspended Sediments (TSS), Total Dissolved Solids (TDS), and Dissolved Organic Carbon (DOC) performed since 1926 at the Brazzaville/Kinshasa gauging station.

The compilation showed that TSS concentrations remained relatively high during the first half of the century and through the wet decades of the 1960s, ranging from 12 mg L^{-1} to 58 mg L^{-1} from 1926 to 1986. [40] Olivry et al. (1988) attributed the dispersed results of earlier studies to the imprecision of measurements. [19] Probst et al. (1992) used stochastic and deterministic methods to estimate 41.61 $\times$ 10^6 t yr^{-1} and 3.41 $\times$ 10^6 t yr^{-1} of dissolved material exported by the Congo and Ubangi rivers 40 km upstream of Brazzaville and at Bangui respectively. They noted that the monthly concentrations of dissolved elements vary inversely with discharge. [13] Moukolo et al. (1993), on the other hand, derived values of 61.1 $\times$ 10^6 t yr^{-1} for the basin outlet from 1987 to 1991, using another method of calculation. For the next few years between 1987 and 1996, monthly sampling and analyses were performed and velocity weighted concentrations of TSS fluxes were computed [41,42] (Olivry et al., 1995; Coynel et al., 2005). The range of TSS fluxes was from 8.3 to 11 t km^{-2} yr^{-1} further highlighting the limited interannual variability of material fluxes in the CRB.

Laraque et al. [9,43] (2009, 2013a) gives a concise review of material export rates at the sub-catchment and whole catchment level respectively. The lack of data for some drainage units was overcome using the principle of similarity-a method that relies on a sound knowledge of the physiographic functioning of the basin. Mean TSS concentrations were also within the range of previous assessments at 25.0 mg L^{-1}. Similarly, [43] Laraque et al. (2013a) obtained, using linear interpolation methods for missing data, average TSS concentrations of 25.4 mg L^{-1} at the basin outlet. [27] Moukandi N'kaya et al. (2020) made a comparison of the variability between two measurement periods: the Programme d'étude de l'Environnement et de la Géosphère Intertropicale-Operation Grands Bassins Fluviaux (PEGI-GBF), and the Observation Service For The Geodynamical, Hydrological and Biogeochemical Control of Erosion/Alteration and Materials Transport in the Amazon, Orinoco, and Congo Basins (SO-HYBAM). They noted a 7.5% increase of TSS (from 30.2 to 33.6 $\times$ 10^6 t yr^{-1}), a 28% increase of DOC, and a 15% decrease in TDS concentration in the current period. They attributed these variations to the increase in water flows since the PEGI period. While these studies have shown the low variability of the material fluxes of the CRB, largely due to its stable and regular hydrological regime, they noticed an increase in the year-to-year variability of TSS concentration, from 25.3 $\pm$ 4.6 mg L^{-1} in 1987–1993 to 27.2 $\pm$ 7.9 mg L^{-1} in 2006–2012. However, there is the need for a more regular monitoring of the river networks with emphasis on the spatial distribution. For now, the only reliable gauge network is at the basin outlet with other sources of data, mainly independent studies conducted by workers for short periods. The obvious impact on this work will be the uncertainties that will arise from this lack of spatial and temporal representation.

2.2. Data and Methodology

The TRMM rainfall product (TMPA) 3B42 V.7 was used to force the SWAT hydrological model. The TRMM product has a spatial resolution of 0.25° and has been validated over the Congo basin by Munzimi et al. (2015) using independent datasets of historical isohyets. Water discharge and suspended sediment measurements from the five principal drainage basins of the Congo basin were obtained from the SO/HYBAM Observatory and its collaborators; notably the CICOS (Commission Internationale du bassin Congo-Oubangui-Sangha), the GIE-SCEVN (Groupement d'Intérêt Economique—Service Commun d'Entretien des Voies Navigables), the RVF (Régie des Voies Fluviales), the PEGI/GBF project, and the Marien N'gouabi University. The 90m resolution SRTM digital elevation model from the consortium from spatial information was used. This resolution was considered considering the size of the basin and the uncertainties related to DEMs [44] (Wechsler et al., 2007). Meteorological data from 1979 to 2014 was provided by the Climate Forecast System Reanalysis (CFSR) and is available at https://swat.tamu.edu/ (accessed on 6 June 2018). Other spatial

data include the 1 km resolution Harmonized World Soil Database [45] (HWSD), while the land cover and land use information was derived from the Global Landcover database 2000. Further details of these inputs and other supporting data used are shown in Table 1.

Table 1. Input data used to run the SWAT model.

Data Type	Period	Resolution	Source
Land elevation		90 m	Digital Elevation Model. Consortium for spatial information (https://cgiarcsi.community/data/srtm-90m-digital-elevation-database) (accesed on the 6 June 2018)
Soil		1 km	Harmonized World Soil Database v 1.1 (http://webarchive.iiasa.ac.at/Research/LUC/External-World-soil-database/HTML/index.html?sb=1) (accesed on the 6 June 2018)
Land use		1 km	Global Land Cover 2000 database (http://forobs.jrc.ec.europa.eu/products/glc2000/products.php) (accesed on the 6 June 2018)
Rainfall	1998–2015	0.25°	TRMM (TMPA) 3B42 V.7 Daily product. Multi-satellite precipitation analysis (https://pmm.nasa.gov/data-access/downloads/trmm#) (accesed on the 6 June 2018), [46] Huffman et al. (2007)
Meteorological data	1979–2014	~38 km	Climate Forecast System Reanalysis (CFSR) Model (http://rda.ucar.edu/pub/cfsr.html&http://globalweather.tamu.edu/) (accesed on the 6 June 2018)
River discharge	2000–2012	Daily	SO-HYBAM (http://www.so-hybam.org/) (accesed on the 6 June 2018); [30] BRLi (2016)
Suspended sediments	2006–2017	Monthly	SO-HYBAM (http://www.so-hybam.org/) (accesed on the 6 June 2018)
			Supporting data
Water productivity	2009–2018	250 m	FAO (https://wapor.apps.fao.org/catalog/WAPOR_2/1) (accesed on the 6 June 2018)
Wetland extent	1992–2000	30 × 30 s	Global Wetlands database, [36] Lehner and Döll (2004) (https://www.worldwildlife.org/publications) (accesed on the 6 June 2018)
Geology	2012	0.5°	Global lithological database [47] (Hartmann and Moosdorf, 2012).

2.3. Modeling Approach

SWAT Model Overview

The Soil and Water Assessment Tool (SWAT) is a semi-distributed, physically-based model capable of integrating various spatial environmental data, including climate, soil, land cover and topographic features. SWAT simulates various hydrological processes e.g., surface runoff, infiltration, evapotranspiration (ET), lateral flow, percolation to shallow and deep aquifers and channel routing [48] (Arnold et al., 2012). SWAT simulates the hydrology of a catchment in two ways: (i) the land phase of the hydrologic cycle and (ii) the channel or routing phase of the hydrological cycle. The first phase controls the amount of water, sediment, nutrients and pesticides loadings to the main channel in each subbasin. The second phase is related to the movement of water, sediments, nutrient and pesticide through the channel network of the watershed to the outlet [49] (Neitsch et al., 2011). More details on the hydrological setup of SWAT for the Congo basin can be found in [50] Datok et al. (2021) and further details of the hydrological processes and equations used for hydrological simulation can be found in the SWAT documentation (https://swat.tamu.edu/; accessed on 6 June 2018).

2.4. SWAT Hydrological Model Setup

The catchment was delineated based on the dominant land use, soil and slope classes apportioning one sub-basin per Hydrologic Response Unit (HRU). This delineation performed within ESRI ArcGIS 10.4 using the ArcSWAT interface (www.esri.com; accessed on 6 June 2018) resulted in 272 subbasins and HRUs with 20 land uses and 14 soil classes (Figure 2a,b). Reservoirs were integrated into the upper part of the Lualaba subbasin to take into account the series of lakes and swamps that act as storages and affect downstream flows. The reservoirs were placed in the outlet of the sub-basins that receive flow from Lakes Tanganyika, Upemba, and Mweru. Reservoir parameters were set according to [50] Datok et al. (2021). Surface runoff was simulated using a modification of the soil conservation service Curve Number (CN) method. The runoff from each sub-basin was routed through the river network to the main basin outlet using the variable storage method. We modelled Evapotranspiration using the Penman–Monteith method. The model was calibrated with measured data on a monthly time scale from 1998 to 2012; comprising calibration (2000–2006), validation (2006–2012), and a two-year warm-up period (1998–2000), to enable the model to achieve a quasi-steady state condition. The criteria of efficiency (NSE) and Kling–Gupta efficiency [51] (Gupta et al., 2009) in 60% of the calibrated and validated stations were above 0.6 and 0.7, respectively, while the percent bias (PBIAS) values ranged from −8 to 8 in all the stations. This result further gave confidence that the hydrology was well simulated, therefore guaranteeing a solid base for estimating soil erosion and sediment dynamics. Further details on the hydrological simulations performed in this case study can be found in [50] Datok et al. (2021).

2.5. SWAT Sediment Model

SWAT uses a Modified Universal Soil Loss Equation (MUSLE) developed by [52] Williams (1975) to simulate sediment yield:

$$\mathrm{Sed} = 11.8 \times (\mathrm{Q_{surf}} \times \mathrm{q_{peak}} \times \mathrm{A_{hru}})^{0.56} \times (\mathrm{C_{USLE}} \times \mathrm{P_{USLE}} \times \mathrm{K_{USLE}} \times \mathrm{LS_{USLE}} \times \mathrm{F_{CRFG}}) \quad (1)$$

where, Sed is the sediment yield on a given day (metric tons day^{-1}); $\mathrm{Q_{surf}}$ = Surface runoff volume (mm day^{-1}); $\mathrm{q_{peak}}$ = runoff peak discharge (m^3 s^{-1}); $\mathrm{A_{hru}}$ = HRU area (ha); C, P, K, LS and F, are non-dimensional factors associated with the crop cover, management practice, soil erodibility, slope and stoniness [53] (Wischmeier and Smith, 1978). The stoniness refers to the fraction of rock fragments at the surface and must be distinguished from rock fragments below the surface. Surface rock fragments affect the C-cover factor, while below surface rock fragments affect the soil erodibility. The MUSLE replaced the rainfall factor (R) of the original USLE [54] (Wischmeier and Smith 1965) with instantaneous peak flows and total runoff to predict soil erosion. Two processes control the sediment transport in the channel network: deposition or erosion. The channel dimensions can either be kept constant so that SWAT can compute deposition/erosion. Otherwise, channel degradation can be activated which would allow channel dimensions to change and be constantly updated as a result of downcutting and widening [49] (Neitsch et al., 2011). In this study, we selected the former option, as the latter has not been proven yet.

Just like the hydrological phase, the sediment phase also consists of the landscape and channel component. SWAT routes different particle sizes through grassed waterways, wetlands/ponds and vegetative filter strips in the land phase. Therefore, the sediment yield reaching the stream channel is the sum of the total sediment yield calculated by MUSLE minus the lag and the impediments listed before [49] (Neitsch et al., 2011). To calculate sediment balance, Sediment from upland sub-basins are routed and added to downstream reaches. This depends on the sediment transport capacity of the reach, which in turn depends on the stream power at the reach. A modified Bagnold's equation is employed to calculate the maximum concentration of sediments that can be transported in the reach:

$$\mathrm{Conc_{max}} = C_{sp} \left(\frac{prf \times q_{ch}}{A_{ch}} \right)^{\mathrm{spexp}} \quad (2)$$

where $Conc_{max}$ = the maximum daily concentration of sediments (t m^{-3}) that can be transported in the reach; *prf* = the sediment peak rate adjustment factor; q_{ch} =average rate of peak flow (m^3 s^{-1}); A_{ch} = channel cross-sectional area (m^2). The coefficients C_{sp} and spexp regulate the linear and exponential relationship between the stream power and the peak velocity and are customized by the user during model calibration. Sediments are deposited when sediment concentration exceeds $Conc_{max}$ (aggradation). Conversely, when sediment concentrations are below the stream transport capacity, nothing is deposited and bed sediment could be eroded if channel erodibility is activated. In this study, channel erodibility was applied sparingly during calibration in selected subbasins. More details of sediment transport equations and processes simulated in SWAT can be found in the SWAT theoretical documentation [49] (Neitsch et al., 2011).

2.6. SWAT Sediment Setup

SWAT2012 and ArcGIS 10.4 were used in this study. As stated earlier, the whole basin was divided into 272 subbasins with 14 land-use classes (Figure 2a) and 20 soil classes (Figure 2b). Only one HRU was defined for each subbasin, based on the combination of the dominant land use and soil type. This was done considering the size of the basin and the computational requirements needed. Furthermore, the MUSLE must be applied to a hydrologically isolated unit for a correct assessment of the water balance [55] (Vigiak et al., 2015). The final range of the HRU area was 0.085–61,775 km^2 with a median value of 9726 km^2. We considered this delineation fit for our purpose, with consideration of our inputs, computational resources and modelling priorities to avoid the risk of misleading results [56] (Jha et al., 2004).

The USLE cover and management factor (C_{USLE}) values were converted from the 14 land uses (Figure 2a) by SWAT based on the amount of soil cover specified for a particular land use, and were extracted from the soil database during model set up. The agricultural area represents a small part of the land use in the basin (<2%) (see Figure 2a), therefore the C_{USLE} and support practice (P_{USLE}) factors were not calibrated and set at default values over this land use. The topographic factor LS_{USLE} is automatically derived from the DEM while the coarse fragment factor (F_{CRFG}) is calculated from the percent of rock in the first soil layer. When there is no rock in the first layer, the F_{CRFG} value is 1.

The soil erodibility factor (K_{USLE}) was carefully calculated over each HRU. This was important in order not to expect too much from default model parameters, and in data scarce basins such as the CRB; a hydrological model should be setup with as much information as available. The default model parameters are based on the Harmonized World Soil Database, and SWAT commonly uses the most dominant soil series in that soil association. The information contained in the database is variable [45] (HWSD), and thus may or may not be representative of the soils in the locality.

The K_{USLE} erodibility factor K was estimated using the freely available software Kuery 1.4 [57,58] (Borselli et al., 2009, 2012). It is based on the equations developed by [59,60] Torri et al. (1997, 2002) from observations of a global dataset of 240 soils where erodibility is expressed as:

$$K = 0.0293\left(0.65 - D_g + 0.24{D_g}^2\right)e^{\{-0.021(\frac{OM}{C}) - 0.00037\,(\frac{OM}{C})^2 - 4.02C + 1.72C^2\}} \quad (3)$$

where *C* is the fraction of total clay content, *OM* is organic matter as a percentage, and D_g is the logarithm of the geometric mean D of the particle size distribution. In cases such as our own, where data of textural components of soil exist only as a percentage; sand (S), loam (L) and clay(C), D_g is calculated according to [61] Shirazi et al. (1988) as:

$$D_g = \frac{-3.5C - 2.0L - 0.5S}{100} \quad (4)$$

As compared to a homogeneous soil, K is affected by the percentage of rock fragment (R_{fg}) in the soil, which is needed as input in Kuery 1.4, as well as the climate classification

of the soils [62] (Salvador Sanchis et al., 2008). In addition, the logarithm of the geometric standard deviation of the geometric mean of the particle size distribution (Sg) [61] (Shirazi et al., 1988) is needed:

$$S_g = \sqrt{\frac{C(-3.5 - D_g)^2 + L(-2.0 - D_g)^2 + S(-0.5 - D_g)^2}{100}} \quad (5)$$

The technical report of the soil and terrain database of the Democratic Republic of the Congo [63] (Engelen & Verdoodt, 2006), the Soil and Terrain Database for Central Africa (SOTERCAF) and the Harmonized World Soil Database [45] (HWSD) were consulted for the basic inputs D_g, S_g, OM, and percentage rock content (R_{fg}). The means of the resulting probability distribution was implemented and spatialized in the SWAT model based on the dominant soil types in the basin (Figure 2b). Table 2 shows the textural components in the percentage of ferralsols used as inputs to the Kuery 1.4 model. Ferralsols are the dominant soil class in the CRB covering 58% of the watershed area as delineated by the SWAT model. Textural components of the ferralsols were obtained based on the soil characteristics of eight locations covered by these soils. Other dominant soil classes with their textural components are shown in Table 3. These eight soil classes make up 40% of the watershed area with watershed size ranging from 0.65% to 17.41%. The textural component percentages of these eight soil classes were obtained from characteristics of these soils and generalized across the basin (Table 3). The climate zone for our study area corresponds to the tropical classification of the Köppen–Geiger climate map of [64] Peel et al. (2007) and identified as such in our study. The generated K values frequency distribution allowed us to choose a more representative value for a given soil based on its characteristics given in our soil databases. These characteristics linked mainly to soil structural stability are derived from the description of soil profiles in the databases and literature.

Table 2. Percentage values and statistics of textural components of ferralsols, which make up 58% of the basin soils, used in the Kuery 1.4 model.

	Sand%	Loam%	Clay%	Organic Matter%
MIN	17.7	17.9	0.8	0.52
MAX	49.9	69.4	36.6	11.1
MEAN	31.20	42.79	22.79	2.35
Std ± (standard deviation)	11.36	18.48	12.07	3.64

Table 3. Values of textural components of other dominant soils in the basin used in the Kuery 1.4 model.

SOIL	Percentage of Watershed Area	Sand%	Loam%	Clay%	Organic Matter%
Acrisols	7.0	60	20	20	0.4
Arenosols	17.41	70	20	10	0.7
Cambisols	6.98	47.9	31.5	20.6	0.46
Gleysols	3.74	10	20	70	7.2
Lixisols	1.21	8.2	44.5	47.3	1.2
Luvisols	0.80	73.8	20.7	5.5	0.18
Nitisols	0.65	10	30	60	2.17
Plinthosols	2.65	52	28	20	0.25

2.7. Sediment Balance

We replicate the approach used by [50] Datok et al. (2021) in their hydrological study to estimate the sediment balance in the Cuvette Centrale. 11 points were selected in the model; eight upstream sub-catchments of River stations with their outlets feeding into the wetlands of the Cuvette Centrale (stations 1 to 8, Figure 3). They were completed by three additional stations: one at the outlet of the Kasai subbasin (st. 10), one at the gauging

station of Brazzaville/Kinshasa (st. 11), and one intermediate station in the Congo River downstream of the wetlands (st. 9). The total input of sediment for the Centrale Cuvette is given by $I = \sum_{i=1}^{8} S_i$, the output is considered as the flux at Brazzaville/Kinshasa minus the contribution of Kasai $O = S_{11} - S_{10}$, and the sediment balance of the Cuvette Centrale is:

$$\Delta S = I - O \quad (6)$$

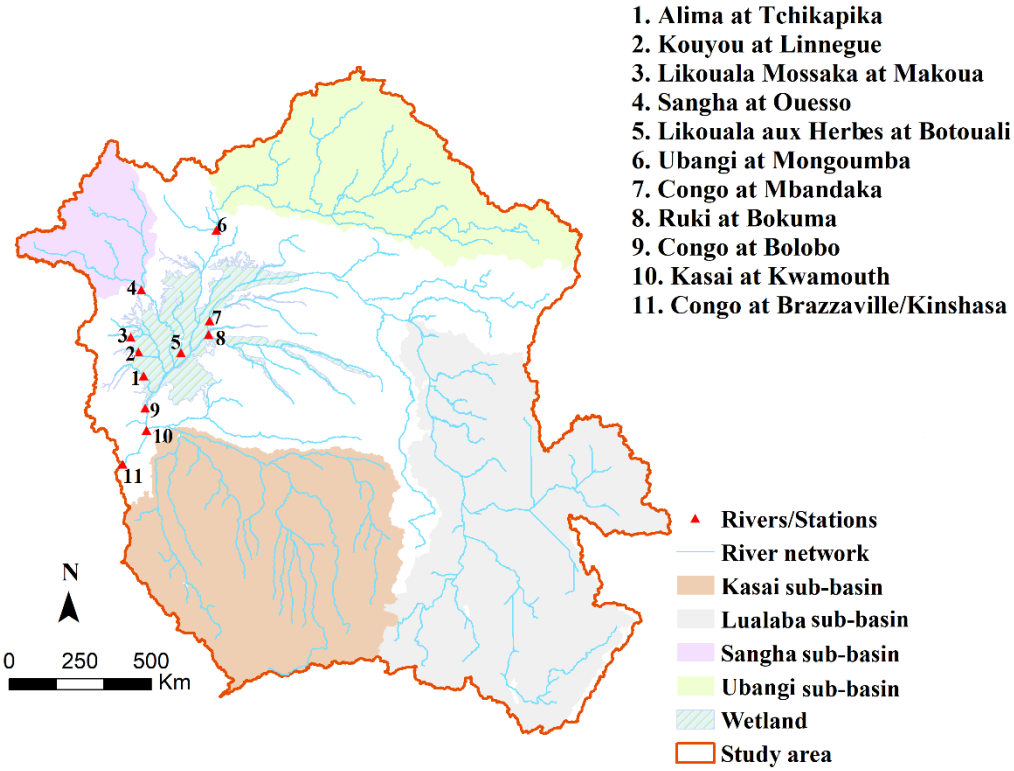

Figure 3. The Congo River Basin showing points used in the calculation of the sediment balance numbered 1 to 11.

2.8. Calibration and Validation of the Model

The hydrological model was validated daily. The model was then calibrated on a daily time-step with suspended sediment (SS) concentration time series (mg L^{-1}). This time series comprises a one to three times monthly sampling obtained from the HYBAM observatory located at the Brazzaville/Kinshasa gauging station. The period of the calibration was 2006 to 2009, while validation was performed from 2010 to 2012. The other only source of SS data that was reliable for use was that measured on the Ubangi River [65,66] (Bouillon et al., 2012, 2014). We used their dataset to calibrate and validate the model at the upstream station on the Ubangi River at Bangui: from March 2010 to March 2011 for calibration, and from April 2011 to March 2012 for validation. The Brazzaville/Kinshasa records used were once-monthly readings from 2006 to 2012 while the measurements on the Ubangi River were based on the 52-day sampling program of [65,66] Bouillon et al. (2012, 2014). Spatialization of the calibration was highly limited due to the lack of gauging stations; therefore, we relied on literature data to calibrate broadly. Manual calibration with the aid of expert knowledge was also used for calibration. Since we lacked critical data for calibration, we first ran our model as simple as possible. We assumed zero net erosion or deposition in the channel by setting the exponential and linear parameters to eliminate deposition and the channel routing parameters to eliminate erosion. We then adjusted the support practice factor that controls the upland sediment yields and calibrated parameters

controlling channel deposition and erosion in an upstream-downstream manner. Details are given in the next section.

Due to the paucity of SS data in this region, the simulated SS concentrations in the period 2000–2012 were validated using historical records measured at the Brazzaville/Kinshasa gauging station from the PEGI/GBF program (1987–1994). The justification for this method is based on the works of [67,68] Laraque et al. (2001, 2013b) and [28] Moukandi et al. (2021), who using statistical tests highlighted the low variability of hydrological regimes during different homogenous periods in the CRB. We selected stations that had at least five months of readings and compared the means noting the assumptions made in comparing the model performance objectively due to the lack of a common frequency of measurement.

2.9. Statistical Analysis

Literature has described the CRB as flat [31] (Daly et al., 1992), with the absence of mountain ranges and thick vegetation cover, resulting in low erosion rates [26] (Laraque et al., 2020). Therefore, a Principal Component Analysis was carried out to identify the most influential factors affecting sediment yield and erosion in the CRB. [69] Vanmaercke et al. (2014) analysed sediment yield in Africa and showed that seismicity, topography, vegetation cover and runoff are the main factors that control sediment yield. Therefore, based on the influence of the parameters analysed in the hydrological simulation in [50] Datok et al. (2021), as well as the well-documented influence of slope and soil on erosion in the CRB [17,39] (Mushi et al., 2019; Kabuya et al., 2020), five variables were incorporated in the PCA. They are the slope in the HRUs (HRU_slp), precipitation (PCP), soil erodibility, (USLE_k), channel vegetation cover (CH_COV2), and surface runoff (SUR_Q). A Pearson correlation was also made between the variables and the most important principle components to measure the strength of their association. These analyses were performed in Rstudio with R version 4.0.

Quantitative means of assessment were also used to evaluate model performance. They include the Nash Sutcliffe efficiency (NSE), the coefficient of determination (R^2) and percentage bias (PBIAS) [70] (Moriasi et al., 2015).

3. Results

3.1. Hydrological Responses in the Main Tributaries

Generally, the model exhibited an acceptable correspondence between the observed and modelled flows, showing its ability to capture the general shape of the hydrograph and magnitude of both high and low flows satisfactorily, at the outlet of the basin as well as in its sub-basins [50] (Datok et al., 2021). The validation of the daily simulations highlighted that SWAT can be calibrated at a monthly time step and validated at a daily time step. The differences in the evaluation criteria show the effect of the regionalization in the calibration as well as the level of complexity of each sub-basin. The lower performance of the daily model compared to the monthly simulation can be linked to the inadequate spatial representation of rainfall as well as errors in other inputs and measurements [71] (Adla et al., 2019). In addition, there are obvious differences between the observation and simulation datasets in both time steps. Much of the discussion about the hydrological responses in the various sub-basins have been documented in [50] Datok et al. (2021). However, to have an overview, we summarize the main points that are essential for the application to sediment modelling.

The Northern sub-basin of the Ubangi, which controls about 16% of the basin, gave good to satisfactory outputs for the evaluation criteria used since it had the most reliable observed data amongst all sub-basins. Therefore, most of the processes operating in the basin were well captured.

The Sangha sub-basin, which is situated west of the Ubangi sub-basin (Figure 1), was also calibrated on a monthly time scale. The model was not able to capture the minor flood phases in July and August, which were amplified on a daily scale. This was put down to

the effect of wetland processes and the inadequacies of the model structure to deal with this. Nevertheless, it reproduced satisfactorily the timing of the hydrograph as well as the water balance components.

In the southwestern Kasai sub-basin, performance ratings ranged from satisfactory to good, with the hydrograph dynamics well captured. The percent bias (PBIAS) in this sub-basin was low, which could be deceptive as the model underpredicted as much as it over-predicted. However, other evaluation criteria (the NSE, R^2), gave a good account of the results here, and the discharge predicted was within three per cent of the observed values.

The challenge was in attenuating the flows from the wetland regions of the basin, specifically in the upper parts of the Lualaba and the central basin. Reservoirs were added to the Lualaba basin to help in trapping the water generated by the large water bodies there. However, we were able to capture satisfactorily the magnitude of flows within one per cent of the observed value.

At the basin outlet, the effect of the convergence of flows from all the contributing tributaries was evident. We were able to reproduce the magnitude of the flows to within 9% of the observed flows. The objective of the study is not to achieve a perfect calibration of the discharge at the outlet, as the challenges have been well documented [72–75] (Chishugi & Alemaw, 2009; Tshimanga et al., 2012, 2014; Munzimi et al., 2019). Rather, the objective is to find a balance between the flows received by the central basin before being impacted by the "Cuvette Centrale" and the flows measured at the basin outlet. Moreover, to achieve this aim using a mass balance approach, observed measurements are available at the outlet for comparison. An analysis of the parameters showed that groundwater parameters were influential all across the basin, with subsurface processes dominating the Sangha and the central basin. The central basin also had the least response to recharge, while the Kasai and Ubangi basins are drawing up more water from the shallow aquifer to the overlying unsaturated zones through deep-rooted vegetation. Some optimal parameters like the canopy interception compared well with physical observations, being higher in areas with more vegetation and lower in less vegetated areas.

In estimating the water balance of the Cuvette Centrale, [50] Datok et al. (2021) found that the main source of Cuvette Centrale waters was from precipitation (31%) with upland runoff contributing approximately equal amounts (33%) for the 2000 to 2012 simulation period. The Ubangi is the largest tributary contributing 16% while the other left bank tributaries contributed a combined 11%. The seasonality of the flows was well captured, with the main flood in December and two smaller floods in March and May. The balance within the Cuvette Centrale is in surplus only during peak floods in October and April and in deficit at all other periods. The regulatory role of the Cuvette Centrale is demonstrated by its ability to augment flows through groundwater and flooded areas to the River. More details of the hydrological model simulation outputs and results can be found in [50] Datok et al. (2021).

3.2. The Calibration Dataset for Sediment Transport and the Model's Calibration Performance

3.2.1. Data Analysis

Figure 4a shows the relationship between the hydrograph and the suspended sediment concentration on the Ubangi River for a one-year period from March 2010 to March 2011. The hydrological regime of the Ubangi is unimodal, with the main flood period from September to November. There is a noticeable lag in the suspended sediments as they follow the discharge, a form associated with a higher concentration-discharge ratio at the rising limb than the falling limb [76] (Megounif et al., 2013), creating a clockwise hysteresis (Figure 4b), described by [77] Laraque and Olivry (1996). The sediment decline at the peak flood is usually attributed to diminishing sediment available in the stream channels [78] (Wang et al., 1998). It must also be noticed that the variability of monthly-suspended sediment concentration (SSC) values is high in the Ubangui basin (from 2.4 to 33.2 mg L^{-1} in 2010–2011).

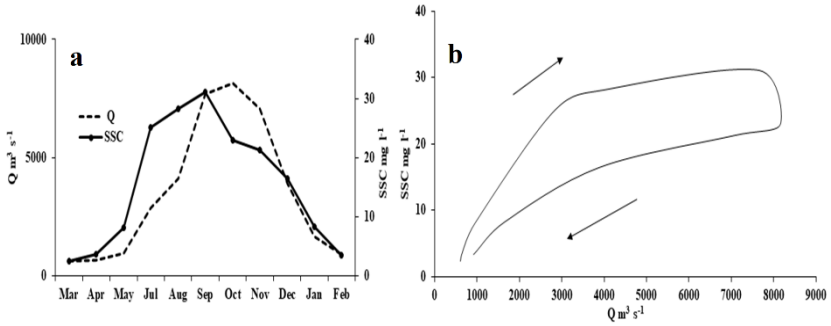

Figure 4. (**a**) The hydrograph and sediment concentration at the Sampling site on the Ubangi River from March 2010 to March 2011 [65] (Bouillon et al., 2012), and (**b**) the resulting hysteresis pattern.

An analysis of the interannual monthly sediment dynamics from 2006 to 2012 at the Brazzaville/Kinshasa gauging station shows the highest concentrations of suspended sediment in March to May at low water while the lowest concentrations are in December/January during the highest peak floods (Figure 5a). [43] Laraque et al. (2013a) also calculated a higher mean monthly concentration of SS of 31.9 mg L^{-1} in March and a lower concentration of 19.1 mg L^{-1} in December for the 2006 to 2010 period. [77] Laraque and Olivry (1996) noted the absence of the erosion-transport-alluvial phases that are associated with the Bangui station. Instead, the Brazzaville/Kinshasa outlet is noted for a single transport phase. This is due to the low seasonal variations in its particulate concentrations and its flows due to the all-year-round contributions of different sub-basins of the watershed to its flow. The hysteresis in Figure 5b displays a figure-eight pattern that combines a clockwise and anti-clockwise stage. This is due to the influence of the two equatorial regimes consisting of the main flood peak and a lesser one. The clockwise stage involves an increase of concentrations from the erosion of initially deposited stream sediments and thereafter a dilution effect with increased discharge [78,79] (Laraque et al., 1995; Aich et al., 2014). The anticlockwise stage follows with decreased discharge and increased sediment concentration on the falling limb. This is due to more available sediment for transport [76] (Megnounif et al., 2013), and in this case, could be related to travel time and contribution of sediment from upstream sub-basins and/or the effect of upstream storages like the Cuvette Centrale [78,80] (Laraque et al., 1995; Malutta et al., 2020). [27] Moukandi N'kaya et al. (2020) analysed the concentration-discharge curves from 2006 to 2017 at the same station and noted a classic dilution pattern of concentration by the discharge with the dilution and concentration effect well marked at the peak and low floods respectively. This figure-eight pattern is common to watersheds like the CRB with at least two distinct flood peaks.

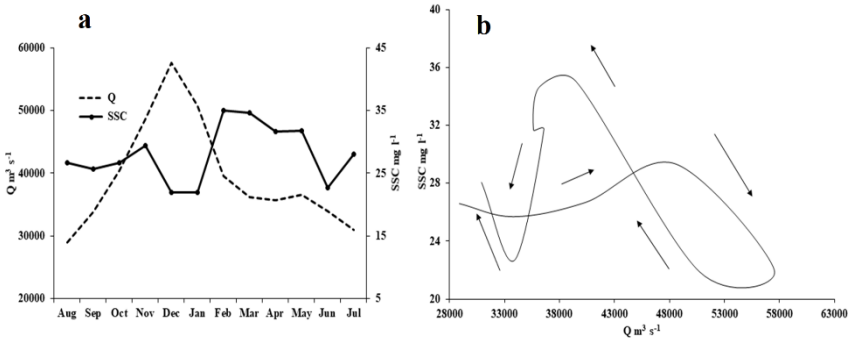

Figure 5. (**a**) The hydrograph and sediment concentration recorded at the Brazzaville/Kinshasa gauging station (2006–2012), and (**b**) the resulting hysteresis pattern.

3.2.2. Calibration Performance

Table 4 shows some parameters used to calibrate sediment dynamics in the SWAT model. The parameters that proved important in the calibration of the sediment yield and

transport are related to the channel processes and processes in the Hydrological Response Units (HRUs). The simulation reveals that the exponential parameter for sediment routing in the channel was the main parameter among the general basin-wide parameters with influence. The values of channel erodibility (CH_COV1) and sediment transport coefficient (SPCON), set to their default values reveal the dominance of channel depositional processes within the basin. The calibration of these factors was done in an upstream-downstream manner. A filter was also implemented in sub-basin 168 corresponding to the confluence of the Kasai with the main river. This was important, as this is a site of deposition due to a change in velocity [17] (Mushi et al., 2019). The length of the filter simulated is 28 m and caused a reduction of about 4% of the total sediment yield at the basin outlet. It is also important to note that the filter strip reduces sediment but does not affect surface runoff [49] (Neitsch et al., 2011).

Table 4. Parameters used to calibrate the sediment model.

Parameters	Description of Parameter	Default	Applied Range
SPEXP	Exponential re-entrainment parameter for channel sediment routing	1	0.5
SPCON (C_{sp})	Linear re-entrainment parameter for channel sediment routing	0.0001	0.0001
PRF	peak rate adjustment factor for sediment routing in main channel	1	1
CH_COV1 (cm^3/N-s)	Channel erodibility factor	0	0–0.02
CH_COV2	Channel cover factor	0	0.65–1
CH_EQN	Simplified Bagnold Equation	0	1
Filter_W (m)	Edge of width filter strip (sub-basin 168)	0	28
LATSED (mg L^{-1})	Concentration of sediment in lateral and groundwater flow	0	50–60
K_{USLE} (t.ha.h./(ha.MJ.mm))	USLE soil erodibility factor	Relative	0–0.04
P_{USLE}	USLE support practice factor	1	1
C_{USLE}	USLE crop cover factor	Relative	0–0.2

Calibration was done at a daily time step at the Bangui station outlet using measured data from the study of [65,66] Bouillon et al. (2012, 2014) from March 2010 to March 2012 (Figure 6a) and at the Brazzaville/Kinshasa station using measured data from SO-HYBAM from January 2006 to December 2012 (Figure 6b). At the Bangui station, the model was able to reproduce the general shape of the hydrograph, capturing both periods of high exports and low exports, a reflection of the good responses already documented during the hydrological calibration and validation at this station [50] (Datok et al., 2021). Statistical metrics used to assess the models' performance are displayed in Table 5. The coefficient of regression of 0.69 showed how much of the variability of the suspended sediments are related to the discharge as the hydrological model has good skill scores. The Nash-Sutcliffe Coefficient of Efficiency (NSE) value of 0.35 is a satisfactory representation of the dynamics captured here when the temporal range of the observed data, as well as the sampling frequency, is considered. In Figure 6a, it can be seen that the simulated load does not follow the observed load during the rising phase of the hydrograph but is more correlated with the discharge at the falling limb. The abnormally high PBIAS value of 49.10 is because of this under-prediction of the rising limb where the magnitudes were not properly captured. Statistics were better in the validation period, with a satisfactory PBIAS value of 24.2%. It is also worth noting that in this sub-basin, the sediment discharge varies over more than two orders of magnitude (2.4–33.2 mg L^{-1} in TSS and 470–8540 m^3 s^{-1} in Q, resulting in a 101–24,508 t day^{-1} range for sediment discharge).

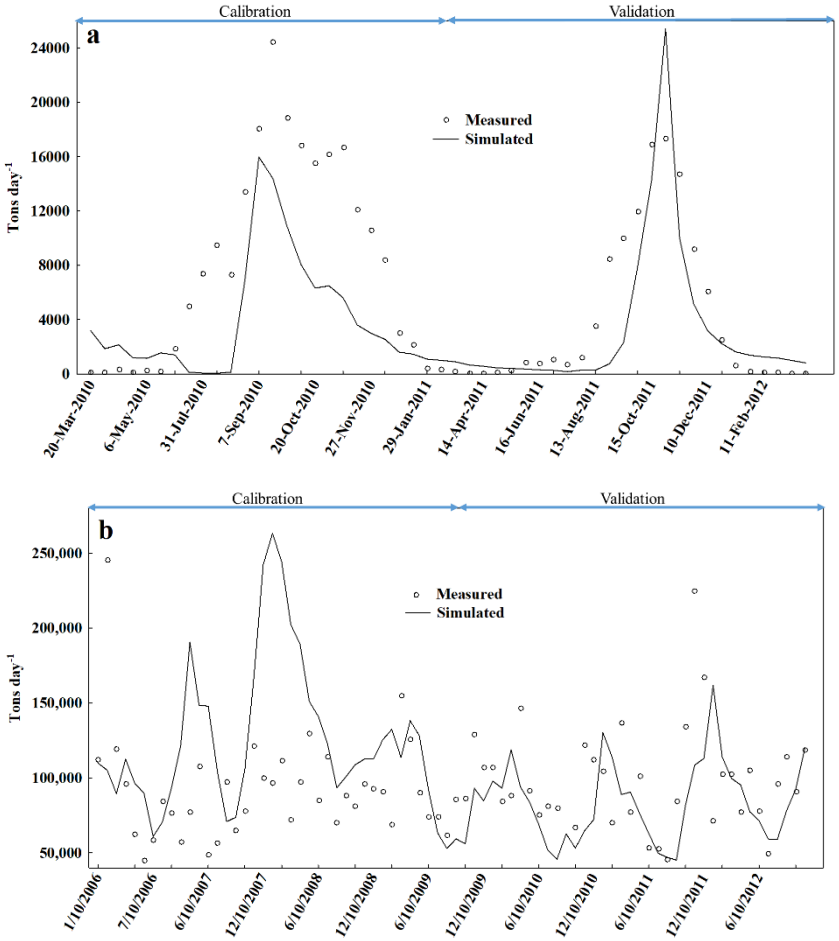

Figure 6. (**a**) Observed and simulated daily sediment fluxes at the northern sub-basin of the Ubangi River before the confluence with the main Congo River data from [65,66] Bouillon et al., 2012, 2014, and (**b**) Observed and simulated sediment fluxes at the basin outlet downstream of the Cuvette Centrale (data from SO-HYBAM).

Table 5. Performance indicators for the daily sediment flux (in t day^{-1}) calibration-validation periods of the model at the Bangui station and the Brazzaville/Kinshasa station.

	Bangui		Brazzaville	
Performance Metrics	**Calibration (2010–2011)**	**Validation (2011–2012)**	**Calibration (2006–2009)**	**Validation (2010–2012)**
NSE	0.35	0.65	−2.95	−0.16
R^2	0.69	0.71	0.02	0.13
PBIAS	49.10	24.20	−29.42	−9.53

Calibration and validation were also performed on a daily scale at the Brazzaville/Kinshasa outlet (Figure 6b). The Brazzaville/Kinshasa gauging station of the CRB receives flow from most of the tributaries that flow into the Cuvette Centrale as well as the Kasai, Plateaux Batekés Rivers and other tributaries downstream of the Cuvette Centrale. The calibration at this point highlights the necessity of a good hydrological calibration to achieve acceptable sediment calibration. Performance indicators at this outlet are −2.95, 0.02 and −29.42 for the NSE, R^2 and PBIAS respectively in the calibration period (2006–2009), while for the validation period (2010–2012), they are −0.16, 0.13, and 9.53 for the NSE, R^2 and PBIAS respectively (Table 5). The NSE is sensitive to extreme flows and reflects the under-prediction of peak flows as well as the influence of the Cuvette Centrale. The low values of regression coefficients also do not give a satisfactory indicator of the

model performance at this outlet as the model did not accurately pick the timing of flows. This is in agreement with what has already been discussed about the failure of models to adequately slow the flow of water across the "Cuvette Centrale" [50,73] (Tshimanga et al., 2012, Datok et al., 2021). Lower statistical performance at Brazzaville Station (Figure 6b) than at Bangui (Figure 6a) also rely on much smaller ranges at Brazzaville (less than one order of magnitude) than at Bangui (more than two orders of magnitude in sediment load). The PBIAS of 9% in the validation period is adjudged satisfactory, however, showing that the model predicted well the average magnitudes although showing a bias towards underestimation of the fluxes.

From the analysis of our calibration dataset and the model calibration, it can be seen that SWAT sediment routing performs better on basins or sub-basins with low or moderate hysteresis (e.g., the Ubangi) than those with high hysteresis (e.g., at Brazzaville/Kinshasa). At Brazzaville, we observe a complex relationship between Q and SSC (figure-eight hysteresis), while the Bagnold formula considers a maximum concentration, increasing with increasing water discharge (or increasing discharge peaks). The difference may be attributed to processes of deposition/erosion over the land (especially in wetlands) or at the riverbed that are very difficult to calibrate correctly over a large basin with a very scarce dataset and natural complexities. To overcome these difficulties, there will be a need for additional measurements in the future at different stations of the basin to improve the model performance. In its state, the model was able to reproduce concentration values and sediment fluxes at a satisfactory level (with PBIAS < 50). It enables the first assessment of sediment balance in the Cuvette Centrale–which is the main target of the paper.

3.3. Additional Comparison of the Model Simulations with Historical Datasets

We compared our simulated fluxes with data from the PEGI-BGF program on the 1987–1994 period since there has not been any sustained sampling program over the entire basin. The justification of this comparison is based on the regularity of measured fluxes in the basin over the past century. For instance, [67] Laraque et al. (2001) highlighted that the hydro-climatology of the basin presented similar 10–12 year cycles in the last half-century. Ref. [81] Nguimalet & Orange (2013) also showed the homogeneity of rainfall-runoff ratios overtime at the Bangui station. Ref. [26] Laraque et al. (2020) showed that the magnitude of the discharge mainly controls suspended sediments due to their weak concentrations, also showing similar temporal variations as the hydrograph. Finally, [27] Moukandi N'kaya et al. (2020) compared the TSS concentrations for 1987–1993 with 2006–2017 values noting insignificant changes and concluded that their concentrations were similar. Simple statistical analysis of the variables in five locations are compared in Table 6. The PEGI observations of SSC and Q were sampled once every month, with some months not sampled at all in some stations, while we used the full time series for the SWAT simulations. More detailed statistical analysis could not be carried out because the frequency of measurement was not the same.

Average SSC values were very well estimated with the model at Bouatali (Likouala aux Herbes River), Ouesso (Sangha River) and Makoua (Likouala Mossaka River), with differences less than 7%, while it was over-estimated by 31.2% at BRZ/Kinshasa (Congo R.), and by 110% at Alima (Tchikapika) (Table 6). Of course, these quantities are not perfectly comparable since simulations ran over years while measurements were performed a limited number of times per station. However, this result confirms the ability of the model to assess a first sediment budget of the Cuvette Centrale.

Table 6. Descriptive statistics comparing suspended sediment concentration and discharge from the PEGI program (1987–1993) and SWAT simulation (2000–2012) from stations within the Cuvette Centrale.

				PEGI/GBF (1987–1993)					SWAT (2000–2012)				Difference between SWAT and PEGI Means (%)
River	**Station**	**#**	**Parameters**	**n**	**Mean ± Std**	**Max**	**Min**	**Max/Min**	**Mean ± Std**	**Max**	**Min**	**Max/Min**	
Alima	Tchikapika	1	SSC	28	7.3 ± 2.63	12.1	3.7	3.27	15.33 ± 1.06	17.06	10.91	1.56	110
			Q	33	553 ± 66.81	660	420	1.57	390 ± 103.91	401	275.8	2.85	29.5
Likouala Mossaka	Makoua	3	SSC	29	13.6 ± 5.77	30.9	3.9	2.95	14.55 ± 2.32	18.51	6.04	3.06	7.0
			Q	33	177 ± 79.73	307	62	3.15	91.55 ± 61.40	543	23.58	23	48.3
Sangha	Ouesso	4	SSC	7	18.5 ± 12.11	38.2	6.6	5.78	24.94 ± 6.57	58.83	15.19	3.87	34.8
			Q	14	1 155 ± 691.77	2920	514	5.68	1106 ± 374.18	4088	630	6.48	4.24
Likouala aux Herbes	Botouali	5	SSC	6	7.71 ± 2.59	11.00	4.60	2.39	7.45 ± 0.94	14.25	4.48	3.18	3.4
			Q	5	412.60 ± 185.18	546.00	134.00	4.07	327 ± 105.2	774	142	5.4	20.7
Congo	BRZ/KIN	11	SSC	99	23.99 ± 5.4	41.2	9.4	4.38	31.48 ± 7.44	78.11	18.66	4.18	31.2
			Q	99	38 515 ± 9642	45,000	37,100	1.21	36,156 ± 8221	64,690	18,430	3.51	6.1

n = number of observations; SSC = suspended sediment concentration (mg L^{-1}); Q = discharge (m^3 s^{-1}); Std = standard deviation; BRZ/KIN = Brazzaville/Kinshasa.

4. Discussion

4.1. Spatial Analysis of SWAT Outputs

4.1.1. Surface Runoff and Sediment Yield

We analysed the spatial variation of sediment yield across the basin (Figure 7). Generally, it can be observed that high surface runoff (Figure 7b) corresponds to high sediment yields (Figure 7a) across the subbasins. Surface runoff also followed the rainfall pattern of the basin with the central areas receiving some of the highest rainfall and above-average sediment yields. The sediment yields are generated from individual HRUs and from Figure 7a, it can be deduced that the Cuvette Centrale area with its various land uses including row cropped fields or pasture is characterized by local erosion. These sediments are generated and then accumulate here, aided by the low slopes and low velocities of water, which combine to restrict the transport of these sediments. The mapped sediment yield rates compare to the ones mapped by [9] Laraque et al., (2009). We estimated sediment yield rates of 4.01, 5.91, 7.88 and 8.68 t km^{-2} yr^{-1} respectively for the Ubangi sub-basin at Bangui, Sangha at Ouesso, Lualaba at Kisangani, and Kasai at Kutu-Moke respectively. The sources of these sediments are mainly from the higher slopes of the eastern highlands, the southern parts of the basin as well as sources from the Angolan highlands to the southwest. These loads are conveyed in the river from the upper course at an altitude of 1400–1500 m and they gather more mass as the river exits the numerous swamps and wetlands in the Lualaba basin. There is a noticeable reduction in river load as it makes its way through the anastomosing river channels of the middle Congo River. These channels are up to 16 km wide at some places [82] (Runge, 2007) and are characterized by sand and silt bars indicating deposition. Effective river width of around 5 km, measured 700 km upstream from Brazzaville/Kinshasa, reduce to less than 3 km at 1600 km upstream as measured by [83] Carr et al. (2019). At the equatorial regions, tributaries from the northern and southern hemispheres join the main river and increase the loads. Some of these loads are contributed by the Ubangi catchment due to the erosion of grazing land of the Sudano Sahelian environment [81] (Nguimalet & Orange, 2013). Water surface slopes are higher here with a reduced velocity. This river stretch is multi-channel with constrictions that reduce the widths considerably [83] (Carr et al., 2019). The Kasai River then joins the main stem at Kwamouth. The Kasai is noted to have a large suspended sediment load [9] (Laraque et al., 2009), contributing to the main river. This is consistent with measurements by [83] Carr et al. (2019) where they found water surface slopes to be very low in this area (2 cm km^{-1}). The loads are then transported and reduced through the Malebo pool with some loads produced at the urban settlement of Brazzaville/Kinshasa.

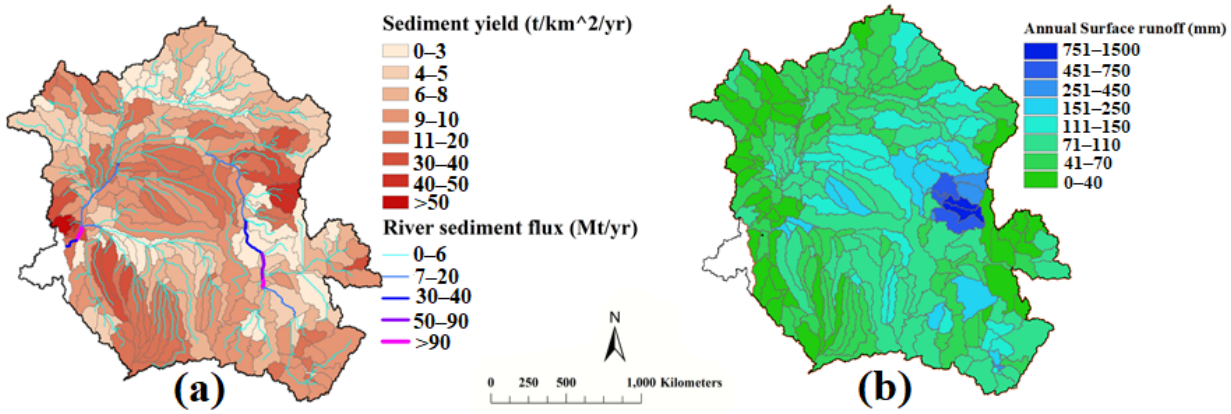

Figure 7. Mean annual variation of (**a**) sediment yield/flux and (**b**) surface runoff in the stream reaches of the CRB for the 2000–2012 period.

4.1.2. Land Use/Land Cover and Sediment Yield

We investigated the relationship between land cover, surface runoff and sediment yield in the CRB sub-basins over different land uses (Figure 8). The dominant land uses are forests, which occur in all the sub-basins while agriculture, pastoralism, and rangeland are the land uses with the most sediment yield.

The Ubangi sub-basin is dominated by forests of the mixed kind, comprising small trees and shrubs, which are interspersed with larger broadleaved trees at the northern limits of the basin. At the lower and wetter parts of the sub-basin are the boundaries of the evergreen forest. The highest yields of 4.5 t km^2 yr^{-1} was in the mixed forests located on higher slopes, while the lowest yield of 2.16 t km^{-2} yr^{-1} was in the evergreen forests. The Ubangi sub-basin presented the lowest specific sediment yield of the principal basins studied. However, in terms of load contribution, it ranks second of the sub-basins that contribute to the Cuvette Centrale after the Lualaba sub-basin. This is mainly because the discharge measured at the Bangui station is the largest of the Northern tributaries. Low sediment yields could also be attributed to the largely stable nature of the Ubangi tree-covered peneplains [17] (Mushi et al., 2019).

The Sangha basin drains the northwestern limits of the CRB; it has relatively high sediment yields compared to its size–5.91 t km^{-2} yr^{-1} (this study) and 8.52 t km^{-2} yr^{-1} [9] (Laraque et al., 2009). The highest yield of sediment is found in pastureland (12.22 t km^{-2} yr^{-1}, see Figure 8) while the evergreen forests produced the least sediment of 3.97 t km^{-2} yr^{-1}. Soils of the exposed pasturelands are more susceptible to erosion than those of the evergreen forests, which are protected by dense tree cover. This is a view held by [84] Ndomba et al. (2011), who also pointed out that agriculture and pastoralism are the main sources of sediment in catchments.

In the Lualaba sub-basin, agriculture is the largest land use by size with the highest sediment yields. Runoff is low though suggesting infiltration of water through the soil profile. Rangeland has a relatively high specific yield of 9.17 t km^{-2} yr^{-1} considering that this land-use ranks fourth in the area behind agriculture, evergreen, and deciduous forests. This may in part be due to overgrazing or other anthropogenic activities that expose the soil. Deciduous forests yielded 7.71 t km^{-2} yr^{-1} of sediment while the evergreen forests yielded 9.68 t km^{-2} yr^{-1} of sediment. The evergreen forests yield the least sediment in the other sub-basins studied. [85] Mayaux et al. (2003) described the evergreen swamp forests as "edaphic", alluding to the influence of the sediments on their sustenance. The trees are also mostly dense and multilayered, helping to slow the agents of erosion. The exception in the Lualaba may be due to the relatively higher slopes in some areas, which induce more yields. Non-forested wetlands yielded 1.25 t km^{-2} yr^{-1} of sediment while wheatgrass yielded 7.39 t km^{-2} yr^{-1} of sediment, noting that, while it is not as high as agricultural output, it shows the effect of different management practices on sediment yield.

The Kasai sub-basin is known to be heavily mineralized, due to the many mining activities taking place there. These anthropogenic activities are very impactful on the land. Therefore, it is not surprising that the highest sediment yields in the CRB are attributed to this sub-basin. We simulated specific sediment yields of 3.8 t km^{-2} yr^{-1}, 11 t km^{-2} yr^{-1}, and 12.7 t km^{-2} yr^{-1} for evergreen forests, deciduous forests, and rangeland, respectively (Figure 8). The sediment yield is more pronounced in the southwestern portion of this sub-basin probably due to anthropogenic activity mentioned earlier and/or less stable natural terrain [17] (Mushi et al., 2019).

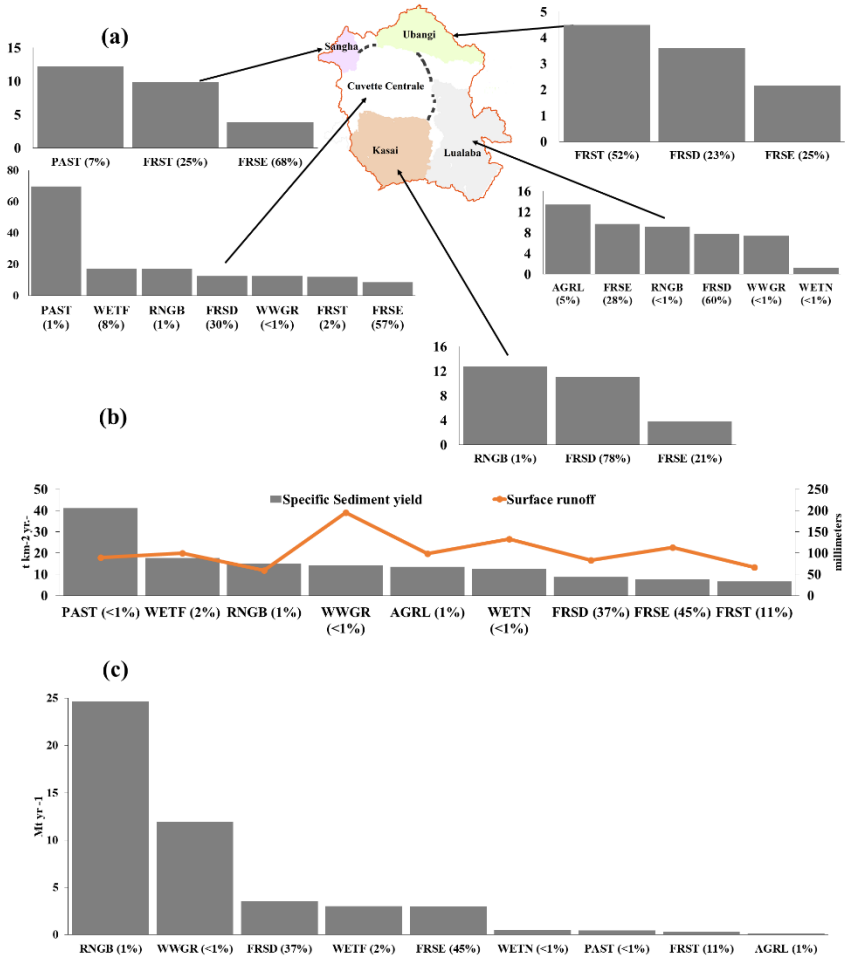

Figure 8. Mean interannual, (**a**) relationship between land cover and the upland sediment yield (t km^{-2} yr^{-1}) in the four subbasins of the CRB and the Cuvette Central area sensu lato (in brackets: percentage of each land cover in the sub-basin). (**b**) Variation of surface runoff with sediment yield (t km^{-2} yr^{-1}), by land use for the 2000–2012 simulation period over the whole basin. (**c**) Annual mean sediment loads produced by different land uses for the 2000–2012 simulation period over the whole basin. Note that the percentage of water bodies as the land cover is not included.

Land cover in the Cuvette is 57% Evergreen forest, 30% Deciduous forest, 8% Wetland forest, 2% Mixed forest with Pasture, Rangeland and Wheatgrass making up the balance. The soils are primarily composed of gleysols, which are affected by groundwater [86] (Ngongo et al., 2014). They are not well-drained and in fact, oversaturated causing relatively high surface runoff. We simulated the highest yields for the Pasture land, Deciduous forests, Wetland forests, Mixed forests, Evergreen forests, and Rangeland of 69, 14.3, 12.13, 12.09, 10.13, and 8.64 t km^{-2} yr^{-1} respectively. In the basin as a whole, high surface runoff

did not necessarily mean high sediment yields, as is the case with wheatgrass. Similarly, mixed forests with the lowest yields (6.5 t km^{-2} yr^{-1}) have only the second-lowest surface runoff rate (66 mm yr^{-1}) (Figure 8b). To put Figure 8a and b in perspective, we plotted the average loads produced by each land use in Figure 8c. From the plot, pastureland, which otherwise has a very high specific yield, actually produced one of the least loads commensurate with its overall percentage of basin area. Likewise for agriculture, mixed forest, and non-forested wetlands.

4.1.3. Sediment Source Areas

Erodibility values calculated with the Kuery 1.4 model are compared with the original SWAT default values in Figure 9a,b The resulting soil erodibility values were a magnitude of 10 less than those estimated by default SWAT values. This is in line with [62] Salvador Sanchis et al. (2008), who showed that soils in warm climates are less erodible than those developed in temperate climates. The map of slope steepness (Figure 9c) also affirms that higher slopes will yield more sediment. Our resulting mapped values compared well with literature, notably the work of [17] Mushi et al. (2019), who used the Global Assessment of Soil Degradation (GLASOD) to map sediment sources within the CRB. Our simulated sediment sources (Figure 9d) is similar to theirs. The results showed that portions of the middle CRB are less affected by erosion, while high relief areas are the primary sources of sediment. It is important to note also the Cuvette central area, although located on low slopes with low erodible soils, yield relatively high sediment within its tributaries because of their high content in organic matter, which are mostly made up of fine particles that are transported easily even at low velocities. The coarser particles, most likely from stream bank erosion, will travel only shorter distances and be deposited, helping to create anastomosing structures observed along the middle reach [83,87,88] (O'Loughlin 2013, 2020; Carr et al., 2019). Thus, a combination of higher rainfall and corresponding surface runoff induced more sediment yield from the Cuvette Centrale. These results would need a thorough field-based verification to compensate for the uncertainties associated with the model, and as [17] Mushi et al. (2019) admitted, the GLASOD map is unable to map all the erosion processes.

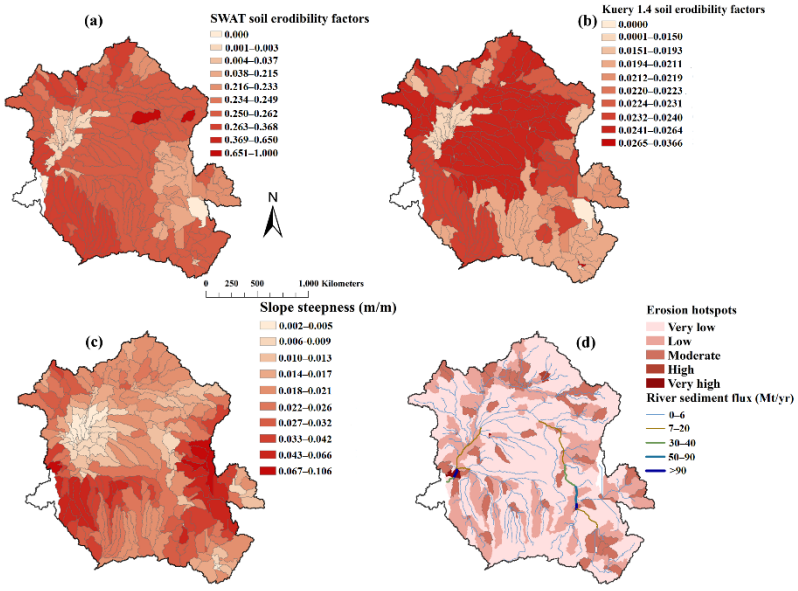

Figure 9. Maps over the Congo River basin comparing the K_{usle} factor calculated with (**a**) SWAT and (**b**) Kuery 1.4, (**c**) slope steepness across the basin and (**d**) areas more prone to soil erosion within the simulation period.

4.2. Key Factors Affecting Sediment Yield

A principal component analysis (PCA) was performed on parameters that affect the sediment yield in the various subbasins of the catchment. Five key parameters were analysed: the slope in the HRUs (HRU_slp), precipitation (PCP), soil erodibility (K_{USLE}), channel vegetation cover (CH_COV2), and surface runoff (SUR_Q). PC1 explained 33.7% of the data variability, while PC2 explained 24.4%. Together, PCA1 and PCA2 accounted for 56.1% of the variability in the data (Table 7). The eigenvalues with the most magnitude in PC1 were 0.66 and 0.58, corresponding to surface runoff and precipitation, respectively. Figure 10a demonstrates this; as values increase positively along the PC1, so does precipitation and surface runoff. In addition, erodibility and slope are moderate and there is less channel cover. Similarly, the eigenvalues with the most magnitude in PC2 are erodibility and the slope in the HRUs with values of −0.62 and −0.59, respectively. Fig. 10b shows that as the values along with PC2 increase negatively, there is a corresponding increase in slope as well as the erodibility of the soils. At the same time, channel cover is low and there is no real difference between precipitation and surface runoff.

Table 7. PCA components and their respective eigenvalues and correlation coefficients.

	PC1	**PC2**	**PC3**	**PC4**	**PC5**	**PC1**	**PC2**
Proportion of variance (%)	33.7	22.4	19.9	16	8	Pearson coefficient	
Cumulative proportion of variance (%)	33.7	56.1	76	92	100		
	Eigenvalues						
HRU_SLP	0.35	−0.59	−0.30	−0.58	−0.31	0.46	−0.62
PCP	0.58	0.41	0.27	0.14	−0.64	0.75	0.43
_K_{USLE}	0.29	−0.62	0.11	0.71	0.07	0.38	−0.66
CH_COV2	−0.15	−0.26	0.90	−0.30	0.01	−0.20	−0.27
SUR_Q	0.66	0.17	0.09	−0.19	0.70	0.86	0.18

To buttress these results, we used the Pearson correlation coefficient to compare the relationship between the variables and our two principal components that explain more than 50% of the data variability. Table 7 shows the highest positive correlation along PC1 of 0.86 associated with surface runoff. This implies that as the value of the observation increases along PC1 so does the surface runoff. Likewise, the next highest value is precipitation (0.75), further reinforcing the dominance of these variables in the CRB sediment processes. The reverse is also true for negative coefficient values; as the value of the principal components increase, the associated variables decrease. Low negative values would also mean negligible relationships between variables as observed with channel vegetation cover in PC1 and PC2.

Our results compare favourably with the literature cited in this study [9,17,39,69,82] (Laraque et al., 2009; Runge et al., 2007; Vanmaercke et al., 2013; Mushi et al., 2019; Kabuya et al., 2020). The principal components can isolate the main factors responsible for the sediment transfer processes in the basin. The regions with relatively higher rainfall and surface runoff, which are the dominant factors along PC1, are situated in the central and highland areas of the east as well as portions of the southwest of the basin. While along PC2, the slope and the erodibility of the soils are closely related. These variables dominate the erosional processes in the highland regions, which surround the basin as well as parts of the main drainage units of the basin. The PCA is also able to group main drainage units with similar characteristics. By condensing our variables into two linear combinations of PC1 and PC2, it will be possible to separate our sub-basins based on the similarity of characteristics. Further work is therefore needed to separate the sub-basins based on the factors influencing erosion. This would need more detailed and extensive data coupled with modelling for a deeper understanding of the sediment dynamics within the CRB.

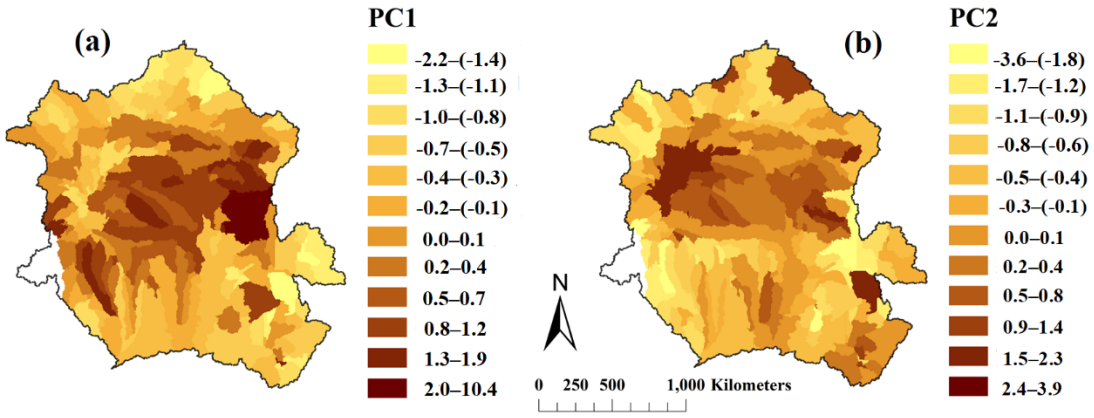

Figure 10. Principal component PC1 (**a**) and PC2 (**b**) values across the CRB simulated with the SWAT model.

4.3. Sediment Balance in the Cuvette Centrale

The Cuvette Centrale acts as a sediment trap slowing the flow of water, nutrients and pollutants [9] (Laraque et al., 2009). To quantify the effects of the Cuvette Centrale on upstream sediment loads, we carried out an upstream-downstream mass balance as described in Section 2.5 and as demonstrated in the hydrological balance of [50] Datok et al. (2021). Eight tributaries from both the northern and equatorial regions were considered and the results of the balance are presented in Table 8 below.

Table 8. Mean yearly simulated averages of suspended sediment fluxes and sediment yield for the 2000 to 2012 period.

Rivers	Contributing Area (km^2)	Station/Town	#	*Annual Load (ton)	% of Total Load Supplied to the Cuvette Centrale	Specific Yield (t km^{-2} yr^{-1})
Congo	1,306,000	Mbandaka	7	*26,981,769*	85.85	20.66
Ruki	163,700	Bokuma	8	*1,602,153*	5.10	9.79
Ubangi	491,800	Mongoumba	6	*1,502,746*	4.78	3.06
Sangha	138,600	Ouesso	4	*942,815*	3.0	6.80
Alima	18,240	Tchikapika	1	*187,469*	0.60	10.28
Kouyou	9631	Linnegue	2	*96,124*	0.30	9.98
Likouala aux Herbes	24,570	Botouali	5	*76,227*	0.24	3.10
Likouala Mossaka	12,240	Makoua	3	*40,495*	0.13	3.31
Congo	2,343,000	Bolobo	9	7,624,230		3.25
Kasaï	778,900	Kwamouth	10	10,503,792		13.49
Congo	3,164,000	Brazzaville	11	37,094,615		11.72

* Values in italics were summed for the total inputs.

We simulated an average of 31.4 million tons of particulate material filling the Cuvette Centrale annually ($I = \sum_{i=1}^{8} S_i$). A large percentage of the fluxes (85%) come from the upper Congo. The Ubangi, the largest tributary of the Congo on the North, contributes about five percent of fluxes while the Ruki, another large tributary with its source in the southern hemisphere also contributes about five percent (Table 8). The Sangha and the other principal tributaries on the right bank contribute three and two per cent to the Cuvette Centrale, respectively.

Compared to the values of 33.7×10^6 t yr^{-1} of material measured by the SO-HYBAM at the basin outlet (station 11) from 2006 to 2017, our simulated value of 37×10^6 t yr^{-1} for 2000 to 2012 compares well. Next, we calculated the fluxes at the confluence of the Kasai River (at Kwamouth; station 10) with the Congo at 10.5 million tons, which was then subtracted from the flux of 37 million tons simulated at the basin outlet resulting in 26.6 million tons of material annually at the basin outlet. With respect to equation 6 in Section 2.7, we estimated the sediment balance as the difference between the fluxes coming

in from stations 1 to 8 (~31Mt) and the fluxes at station 11 (~26 Mt) for a balance of ~5 Mt. To verify the balance, we calculated the fluxes downstream of the Cuvette at Bolobo, which is 7.6 million tons of material. By subtracting the value at Bolobo from the inputs into the Cuvette Centrale gave a value of over 23 million tons, we confirmed that there is a massive reduction in the fluxes exiting the Cuvette Centrale. These high loads retained by the cuvette can be justified by the sediment yields simulated in Figure 7 as well as the anastomosing structures with low velocities (0.75–0.95 m s^{-1}) observed by [83] Carr et al. (2019) which are conducive for sediment storage. [89] Molliex et al. (2019) also suggested that the Cuvette Centrale, including the lakes Tumba and Mai-Ndombe, trap a huge part of the CRB sediment load. [90] Garzanti et al. (2019) from petrographic evidence, suggests that pure quartzite is generated only in the Cuvette Centrale and that the Cuvette Centrale is a quartz factory with a huge reservoir. They also estimated that the Congo is the largest River on Earth carrying pure quartzite to the Atlantic. Coynel et al. (2005) estimated that more than 11 megatons of suspended sediments are exported from only the Savannah areas of the CRB with around 23% of that amount unaccounted for at the basin outlet. While there is no substitute for field-based verification, these studies suggest that the Cuvette Centrale can store such amounts.

Therefore, for the period 2000 to 2012, we estimated that the Cuvette Centrale retained over 23 megatons of material or 75% of the sediment fluxes from 70% of the basin area above Brazzaville/Kinshasa (combined contributing areas of stations 1 to 8). The low velocities observed in this area of the wetlands [83,91] (Laraque et al., 1998a; Carr et al., 2019) would ensure deposition takes place. This would imply a minimum exchange of material between the wetland and the main river. [50] Datok et al. (2021) analysed the water balance of the Cuvette Centrale and verified its role as a sponge or buffer that accumulates water in the rainy season and releases it in the dry season. A running hypothesis suggests that this may be the main means by which supplies–if any–of suspended sediment is made to the main river [33] (Alsdorf et al., 2016). Dilution and concentration effects have also been observed at the peak and low of discharge, respectively [27] (Moukandi N'kaya et al., 2020). This is expected as it has been observed that increasing rainfall increases the specific discharge causing dilution of suspended matter [9] (Laraque et al., 2009). [91] Laraque et al. (1998a) described the hydrological functioning of the floodable parts of the Cuvette Centrale as mainly through vertical exchanges. Thus, coupled with the flat topography and limited lateral exchanges, there is poor mineralization. These characteristics can also be extended to the Lake regions on the left bank of the Congo River i.e., Lakes Tumba and Mai Ndombe, which are located within seasonally inundated forests. They are reservoirs of organic material due to the forest cover and their biogeochemistry is similar to the flooded portions of the Cuvette Centrale.

The seasonal dynamics of the loads contributed to the Cuvette Centrale (Figure 11) show that the right bank tributaries (stations 1–6; Table 8) contribute more load during the September-October-November (SON) floods associated with the equatorial regions. Disregarding the contributions from the main-stem Congo River (station 7); it is obvious that the right bank tributaries are a very important source of sediment to the Cuvette Centrale. This is especially so since unlike the Amazon which has numerous connecting pathways or "furos" between the main river and the floodplains, there is limited connectivity in the case of the CRB [33] (Alsdorf et al., 2016). The left bank tributary (station 8) also makes a modest contribution in the December-January-February (DJF) period that coincides with the small dry season of the southern basins and the pronounced dry season of the northern basins.

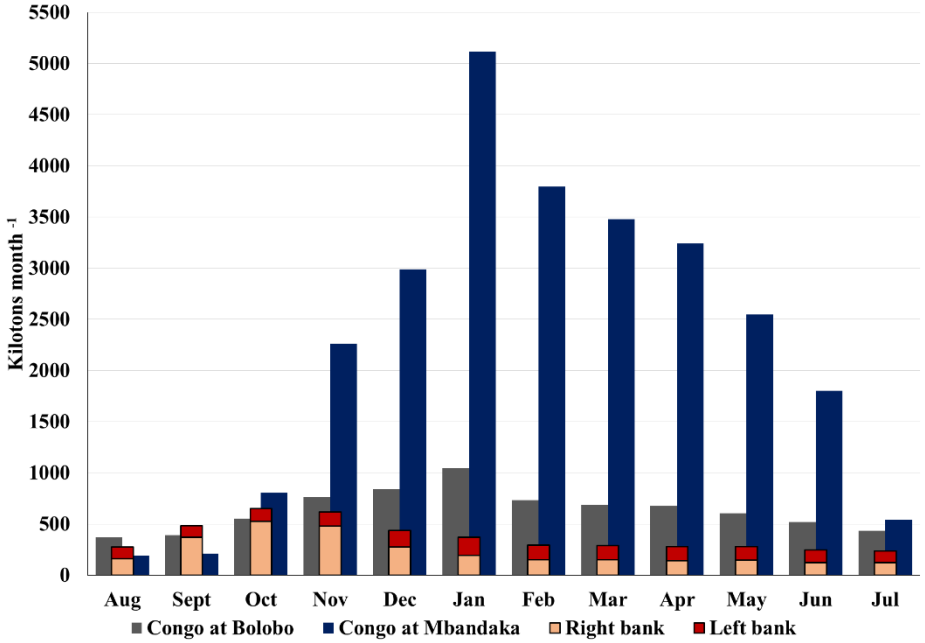

Figure 11. Mean interannual seasonal dynamics of the loads contributed to the Cuvette Centrale from tributaries on the right (Alima, Kouyou, Likouala Mossaka, Sangha, Likouala aux Herbes, Ubangi) and left (Ruki) of the main river, as well as the loads coming in and carried away from the area (Congo at Mbandaka and Bolobo, respectively).

4.4. Comparison with the Amazon and the Orinoco

To put this study in context and appreciate the functioning of the CRB, we compare the material fluxes of the CRB with two other large world drainage basins: the Amazon and the Orinoco. This comparison is important because, after the Amazon, the Congo is the second largest area of tropical rainforest at 1.8 million km^2 [92] (Haensler et al., 2013); and its average discharge of 36,150 m^3 s^{-1} (this study) is second to the Amazon with 169,000 m^3 s^{-1} [93] (Filizola & Guyot, 2009) (Table 9). In comparison to the Orinoco, their mean annual discharges are similar, with the Orinoco discharging 31,400 m^3 s^{-1}. Together, the three river basins combine an average discharge of approximately 284 $\times$ 10^3 m^3 s^{-1} of water into the Atlantic [43] (Laraque et al., 2013). The sediment fluxes reported in Table 9 for the Amazon are taken from the Obidos station that controls 80% of the basin. In terms of the fluxes, both the Amazon and the Orinoco have much higher amounts discharged to the oceans. This is principally due to the difference in relief compared to the Congo as the South American rivers are underlain in part by the Andes [94] (Meade, 1984). In the Congo, chemical weathering dominates over physical weathering with dissolved matter superseding suspended sediments [27,43] (Laraque et al., 2013a; Moukandi N'kaya et al., 2020). The reverse is the case for the Orinoco; due to the influence of mountain chains on discharge and fluxes, the differences in the hydrological regimes, forest cover, and the high seasonal variability of discharge compared to the Congo [43,95] (Richey et al., 1986; Laraque et al., 2013a).

Table 9. Comparison of the discharge and Suspended sediment fluxes in three of the world's largest river basins.

	Congo at BRZ/KIN (This Study)	**Orinoco at Ciudad Bolivar (Laraque et al., 2013a [43])**	**Amazon at Obidos (Filizola & Guyot, 2009 [93])**
Q (m^3 s^{-1})	36,150	31,400	169,000
SSC (mg L^{-1})	31.48	73.9	-
SS load (10^6 t yr^{-1})	37.0	74.0	555
SS yield (t km^{-2} yr^{-1})	11.72	88.5	120

4.5. Uncertainties Related to Sediment Estimation

As with any large scale hydrological modelling study in ungauged basins, uncertainties are unavoidable. In this study, a lack of critical data for calibrating the sediment fluxes caused the model to be calibrated in a lumped manner. There is an unavoidable loss of information caused by the lack of spatial representation. However, the temporal variability was well captured and the magnitude of fluxes matched the literature. It should also be noted that concerns have been raised about the misrepresentation of wetland processes due to gaps in the model structure [50] (Datok et al., 2021). Therefore, this study was undertaken assuming that the processes occurring in the wetlands are straightforward. There is also uncertainty related to input data. For example, the soil database used to construct the SWAT lookup tables was primarily prepared for agricultural use with soil depths not exceeding 100 cm. Therefore, peak flows could be over-simulated in deeper soils resulting in an overestimation of sediment. The DEM resolution for computing the hillslope length also has implications for runoff and erosion computations. The Bagnold equation used to calculate the maximum amount of sediment transported in a stream segment has its limitations [96] (Wei et al., 2020). The algorithm does not differentiate between particle sizes and offers no distinction between channel and flood plain deposition [49] (Neitsch et al., 2011). Precipitation input uncertainty and the uncertainties of parameters of the central basin all have to be taken into account too.

In estimating the sediment balance of the Cuvette Centrale, an analysis of stream hydraulics will also help in determining if the widths and depths of the tributaries studied can process the amounts of sediment over the period considered. Settling rates of sediment in the Cuvette Centrale will also need to be studied. This is important in order not to overlook the possibility that the Cuvette Centrale is subsiding at a rate equivalent to the trapping of the sediments. This is an area of future work that will need exploring.

The existing dams that could affect our results are the Mobayi Dam downstream of the Uele River with an installed capacity of 11.5 MW and the Imboulou Dam on the Lefini River with an installed capacity of 120 MW. In the case of the former, it is upstream of the Bangui station and for the latter, it is downstream of the Cuvette Centrale. The Lualaba basin has swamps and lakes that serve as natural reservoirs with a few man-made ones. However, reservoirs were also integrated into the model to account for these structures. Considering the scale of the study, these effects although negligible, will be a source of uncertainty.

5. Conclusions

Understanding the sediment dynamics in wetlands is important to assess changes taking place over time correctly. These changes could be natural or human-made and could have important ecological as well as socio-economic consequences. We used the SWAT hydrological model in this study to investigate and quantify sediment fluxes and budgets from seasonal to annual time scales using freely available datasets. The SWAT model satisfactorily captured the dynamics of sediment yields and fluxes when compared to past studies. In summary, we have been able to use the SWAT model to do the following:

I. Run the SWAT model on a daily timescale, calibrating the hydrology and sediment dynamics for the 2000 to 2012 period. Five principal catchments of the CRB were calibrated for hydrology based on previous work [50] (Datok et al., 2021). Due to lack

of data, we were only able to calibrate one station in the upper part of the basin as well as the outlet of the basin for the sediments. We achieved acceptable results based on the performance of the evaluation criteria used in the study. For hydrology, the coefficients of efficiency were above 70% in 60% of the sub-basins calibrated, while other evaluation criteria also gave a good picture of the model performance.

II. An assessment of the model outputs revealed that agriculture and pasture were the main land uses with the potential to contribute the most sediment yield. The absence of any major infrastructure like dams in most of the tributaries, to trap sediment even temporarily, makes this an important source of sediments. Generally, the steepest areas of the basin produced more sediment and runoff. Our map of degradation hotspots also revealed that the middle basin is least affected by erosion with degradation more pronounced in the outer rim of the Cuvette Centrale. At the same time, the Cuvette Centrale area showed the lowest values of soil erodibility mainly because of the soil properties. Thus, the erosion within this area is mainly local with corresponding sediment accumulation. The highest specific sediment yields by sub-basin were from the Kasai, aided by intense anthropogenic disturbances that lead to deforestation and degradation of uncovered land. The Ubangi subbasin, on the other hand, an old erosional surface, has the lowest specific sediment yields. In terms of load carried in stream channels, the heaviest loads were carried from the lakes at the southeastern parts of the basin and the confluence of the Kasai with the main Congo River.

III. Principal component analysis revealed the main factors that aid in sediment transport. They include surface runoff, precipitation, the slope in the HRU and the erodibility of the soils. These factors are closely related to the climate and physiography of the catchment with high relief areas more prone to erosion and the high precipitation causing increased surface runoff in the central basin.

We estimated the balance of fluxes entering and exiting the Cuvette Centrale from eight principal tributaries that contribute to the main river. Our estimates suggest that the Cuvette Centrale is indeed a giant reservoir that retains at least 23 megatons of material annually. Sediment from the upper Congo is the main contributor with 85% of the fluxes, while the principal tributary of the right bank- the Ubangi- contributes 5%. The Ruki also contributes about 5%, while the other right bank affluents contribute the remainder. With the lack of a robust database over the entire basin, the results over those areas were measured data are available, provide a higher degree of confidence. More advanced validations are needed over the ungauged portions especially at Mbandaka station as the upper Congo is the main supplier of sediments to the Cuvette Centrale.

This work also showed that the estimation of soil erodibility should not only depend on lithological information or a geological map. This is because their reliability is variable and could lead to over or under-estimates of the K values. Future improvements to the model will focus on the spatial representativeness of the sedimentation processes as well as the use of high-resolution input data. Incorporation of a wetland module will also aid in a proper understanding of the processes in the central ungauged basin (e.g., [97–99] Hughes et al., 2014; Sun et al., 2016, 2018).

This study is a follow-up to [50] Datok et al., (2021), where a water balance of the Cuvette Centrale was made. They found that as much water passed through the Cuvette Centrale from the upper Congo as efficient precipitation falling over the area. Similarly, we estimated that a majority of the fluxes come from the upper Congo. The implications are that sediment, nutrients and pollutants are supplied to the Cuvette Centrale provided there are connecting pathways or overflows from the banks [33] (Alsdorf et al., 2016). The relatively higher water surface slopes in the middle reach passing through the Cuvette Centrale make this a real possibility. Sediment loads and yields are majorly influenced by land cover and land use, which alters upland erosion processes [96,100] (Wei et al., 2020; Sok et al., 2020). Rapid urbanization, hydroelectric dam construction and/or future water diversion schemes would also have a significant effect on the fluxes of material in

the Cuvette Centrale. The consequences on downstream communities of wetland loss and nutrient imbalance from sedimentation are severe and should be given more attention.

For the first time, we have estimated the fluxes trapped by the Cuvette Centrale using an upstream-downstream mass balance approach. Our model can be used as a baseline for future sediment studies of the CRB. Different modelling approaches can also be initiated for the Cuvette Centrale from the point scale to the macro-level and vice versa to understand the processes operating within. Concerted joint efforts by stakeholders are also required if progress is to be made in fully appreciating the functioning of this still, relatively pristine watershed.

Author Contributions: Conceptualization, P.D., S.S. and J.-M.S.-P.; methodology, P.D., S.S. and J.-M.S.-P.; software, P.D., S.S., C.F. and J.-M.S.-P.; validation, P.D., S.S., C.F., A.L., S.O. and J.-M.S.-P.; formal analysis, P.D., S.S., C.F., A.L., S.O. and J.-M.S.-P.; investigation, P.D., S.S., C.F., A.L., S.O. and J.-M.S.-P.; resources, P.D., S.S., C.F., A.L., S.O., G.M.N. and J.-M.S.-P.; data curation, P.D., A.L. and G.M.N.; writing–original draft preparation, P.D.; writing–review and editing, P.D., S.S., C.F., A.L., S.O. and J.-M.S.-P.; visualization, P.D., S.S., C.F., A.L., S.O., G.M.N. and J.-M.S.-P.; supervision, P.D., S.S. and J.-M.S.-P. All authors have read and agreed to the published version of the manuscript.

Funding: This research received no external funding.

Institutional Review Board Statement: Not applicable.

Informed Consent Statement: Not applicable.

Acknowledgments: The first Author wishes to thank the TETFUND for funding his stay at the Laboratoire Ecologie Fonctionnelle et Environnement, Université de Toulouse.

Conflicts of Interest: The authors declare no conflict of interest.

References

1. Hay, W.W. Detrital sediment fluxes from continents to oceans. *Chem. Geol.* **1998**, *145*, 287–323. [CrossRef]
2. Walling, D. Human impact on land–ocean sediment transfer by the world's rivers. *Geomorphology* **2006**, *79*, 192–216. [CrossRef]
3. Haddadchi, A.; Ryder, D.; Evrard, O.; Olley, J. Sediment fingerprinting in fluvial systems: Review of tracers, sediment sources and mixing models. *Int. J. Sediment Res.* **2013**, *28*, 560–578. [CrossRef]
4. NKounkou, R.-R.; Probst, J.-L. Hydrology and geochemistry of the Congo river system. *SCOPE/UNEP-Sonderband* **1987**, *64*, 483–508.
5. Walling, D.E. *The Impact of Global Change on Erosion and Sediment Transport by Rivers: Side Publications Series The United Nations World Water Development Report 3*; United Nations World Water Assessment Program: Paris, France, 2009; Volume 81, p. 26.
6. Mitsch, W.J.; Gosselink, J.G. *Wetlands*, 5th ed.; John Wiley & Sons, Inc.: Hoboken, NJ, USA, 2015.
7. Gosselink, J.G.; Turner, R.E. The role of hydrology in freshwater wetland ecosystems. In *Freshwater Wetlands: Ecologicalprocesses and Management Potential*; Good, R.E., Whigham, D.F., Simpson, R.L., Eds.; Academic Press: New York, NY, USA, 1978; pp. 63–78.
8. Novitzki, R.P. Hydrologic characteristics of Wisconsin's wet-lands and their influence on floods, stream flow, and sediment. In *Wet-Land Functions and Values: The State of Our Understanding*; Greeson, P.E., Clark, J.R., Clark, J.E., Eds.; American Water Resources Association: Minneapolis, MN, USA, 1979; pp. 377–388.
9. Laraque, A.; Bricquet, J.P.; Pandi, A.; Olivry, J.C. A review of material transport by the Congo River and its tributaries. *Hydrol. Process.* **2009**, *23*, 3216–3224. [CrossRef]
10. Mitsch, W.J.; Bernal, B.; Hernandez, M.E. Ecosystem services of wetlands. *Int. J. Biodivers. Sci. Ecosyst. Serv. Manag.* **2015**, *11*, 1–4. [CrossRef]
11. Dargie, G.C.; Lewis, S.L.; Lawson, I.T.; Mitchard, E.T.A.; Page, S.E.; Bocko, Y.E.; Ifo, S.A. Age, extent and carbon storage of the central Congo Basin peatland complex. *Nat. Cell Biol.* **2017**, *542*, 86–90. [CrossRef] [PubMed]
12. Harenda, K.M.; Lamentowicz, M.; Samson, M.; Chojnicki, B.H. The Role of Peatlands and Their Carbon Storage Function in the Context of Climate Change. In *Interdisciplinary Approaches for Sustainable Development Goals*; Springer: Cham, Switzerland, 2018; pp. 169–187. [CrossRef]
13. Moukolo, N.; Laraque, A.; Olivry, J.C.; Bricquet, J.P. Transport en solution et en suspension par le fleuve Congo (Zaïre) et ses principaux affluents de la rive droite. *Hydrol. Sci. J.* **1993**, *38*, 133–145. [CrossRef]
14. Gaillardet, J.; Dupré, B.; Allègre, C.J. A global geochemical mass budget applied to the Congo basin rivers: Erosion rates and continental crust composition. *Geochim. Cosmochim. Acta* **1995**, *59*, 3469–3485. [CrossRef]
15. Dupré, B.; Gaillardet, J.; Rousseau, D.; Allègre, C.J. Major and trace elements of river-borne material: The Congo Basin. *Geochim. Cosmochim. Acta* **1996**, *60*, 1301–1321. [CrossRef]
16. Guyot, J.L.; Olivry, J.C.; Laraque, A.; Orange, D. Discharge and Suspended Sediment Fluxes in Large Tropical Rivers. In Proceedings of the IGBP Synthesis Workshop, Stockholm, Sweden, 1 February 2000; pp. 1992–1994.

17. Mushi, C.; Ndomba, P.; Trigg, M.; Tshimanga, R.; Mtalo, F. Assessment of basin-scale soil erosion within the Congo River Basin: A review. *Catena* **2019**, *178*, 64–76. [CrossRef]
18. Probst, J.L. Carbon River Flues and Weathering CO_2 Consumption in the Congo and Amazon River Basins. *Appl. Geochem.* **1983**, *9*, 1–13. [CrossRef]
19. Probst, J.-L.; Nkounkou, R.-R.; Krempp, G.; Bricquet, J.-P.; Thiébaux, J.-P.; Olivry, J.-C. Dissolved major elements exported by the Congo and the Ubangi rivers during the period 1987–1989. *J. Hydrol.* **1992**, *135*, 237–257. [CrossRef]
20. Seyler, P.; Coynel, A.; Moreira-Turcq, P.; Etcheber, H.; Colas, C.; Orange, D.; Bricquet, J.-P.; Laraque, A.; Guyot, J.L.; Olivry, J.-C.; et al. Organic Carbon Transported by the Equatorial Rivers: Example of Congo-Zaire and Amazon Basins. *Soil Eros. Carbon Dyn.* **2005**, 255–274. [CrossRef]
21. Gumbricht, T.; Roman-Cuesta, R.M.; Verchot, L.; Herold, M.; Wittmann, F.; Householder, E.; Herold, N.; Murdiyarso, D. An expert system model for mapping tropical wetlands and peatlands reveals South America as the largest contributor. *Glob. Chang. Biol.* **2017**, *23*, 3581–3599. [CrossRef] [PubMed]
22. Nguimalet, C.-R.; Orange, D. Caractérisation de la baisse hydrologique actuelle de la rivière Oubangui à Bangui, République Centrafricaine. *Houille Blanche* **2019**, 78–84. [CrossRef]
23. Aagaard, T.; Hughes, M. *10.4 Sediment Transport*; Elsevier BV: Amsterdam, The Netherlands, 2013; Volume 10, pp. 74–105.
24. Oeurng, C.; Sauvage, S.; Coynel, A.; Maneux, E.; Etcheber, H.; Sánchez-Pérez, J.-M. Fluvial transport of suspended sediment and organic carbon during flood events in a large agricultural catchment in southwest France. *Hydrol. Process.* **2011**, *25*, 2365–2378. [CrossRef]
25. Guan, Z.; Tang, X.-Y.; Yang, J.E.; Ok, Y.S.; Xu, Z.; Nishimura, T.; Reid, B.J. A review of source tracking techniques for fine sediment within a catchment. *Environ. Geochem. Health* **2017**, *39*, 1221–1243. [CrossRef] [PubMed]
26. Laraque, A.; N'Kaya, G.D.M.; Orange, D.; Tshimanga, R.; Tshitenge, J.-M.; Mahé, G.; Nguimalet, C.R.; Trigg, M.A.; Yepez, S.; Gulemvuga, G. Recent Budget of Hydroclimatology and Hydrosedimentology of the Congo River in Central Africa. *Water* **2020**, *12*, 2613. [CrossRef]
27. Moukandi, G.D.N.; Orange, D.; Murielle, S.; Padou, B.; Datok, P.; Laraque, A. Temporal Variability of Sediments, Dissolved Solids and Dissolved Organic Matter Fluxes in the Congo River at Brazzaville/Kinshasa. *Geosciences* **2020**, *10*, 341.
28. Moukandi, G.D.N.; Laraque, A.; Paturel, J.; Gulemvuga, G.; Mahé, G. A New Look at Hydrology in the Congo Basin, Based on the Study of Multi-Decadal Chronicles. In *Congo Basin Hydrology, Climate, and Biogeochemistry: A Foundation for the Future*; Geophysical Monograph Series; Alsdorf, D., Moukandi, G., Tshimanga, R., Eds.; John Wiley & Sons Inc.: Hoboken, NJ, USA, 2021. [CrossRef]
29. BRLi. Développement et mise en place de l'outil de modélisation et d'allocation des ressources en eau du Bassin du Congo. In *Rapport Technique de Construction et de Calage du Modèle*; CICOS: Kinshasa, Republic of the Congo, 2016.
30. Kadima, E.; Delvaux, D.; Sebagenzi, S.N.; Tack, L.; Kabeya, S.M. Structure and geological history of the Congo Basin: An integrated interpretation of gravity, magnetic and reflection seismic data. *Basin Res.* **2011**, *23*, 499–527. [CrossRef]
31. Daly, M.C.; Lawrence, S.R.; Diemu-Tshiband, K.; Matouana, B. Tectonic evolution of the Cuvette Centrale, Zaire. *J. Geol. Soc.* **1992**, *149*, 539–546. [CrossRef]
32. Laraque, A.; Mietton, M.; Olivry, J.C.; Pandi, A. Influence Des Couvertures Lithologiques et Végétales Sur Les Régimes et La Qualité Des Eaux. *J. Water Sci.* **1998**, *11*, 209–224.
33. Alsdorf, D.; Beighley, E.; Laraque, A.; Lee, H.; Tshimanga, R.; O'Loughlin, F.; Mahé, G.; Dinga, B.; Moukandi, G.; Spencer, R.G.M. Opportunities for hydrologic research in the Congo Basin. *Rev. Geophys.* **2016**, *54*, 378–409. [CrossRef]
34. Bwangoy, J.-R.B.; Hansen, M.C.; Roy, D.P.; De Grandi, G.; Justice, C.O. Wetland mapping in the Congo Basin using optical and radar remotely sensed data and derived topographical indices. *Remote Sens. Environ.* **2010**, *114*, 73–86. [CrossRef]
35. Lehner, B.; Döll, P. Development and validation of a global database of lakes, reservoirs and wetlands. *J. Hydrol.* **2004**, *296*, 1–22. [CrossRef]
36. Crosby, A.G.; Fishwick, S.; White, N. Structure and evolution of the intracratonic Congo Basin. *Geochem. Geophys. Geosystems* **2010**, *11*, 1–20. [CrossRef]
37. UNESCO. Resources of the World and Their Use. 2004. Available online: https://unesdoc.unesco.org/ark:/48223/pf0000134433 (accessed on 4 February 2021).
38. Le Heron, D.P. *Schlüter, T. Geological Atlas of Africa, with Notes on Stratigraphy, Economic Geology, Geohazards and Geosites of Each Country*; Springer: Berlin/Heidelberg, Germany, 2006. [CrossRef]
39. Kabuya, P.M.; Hughes, D.A.; Tshimanga, R.M.; Trigg, M.A.; Bates, P. Establishing uncertainty ranges of hydrologic indices across climate and physiographic regions of the Congo River Basin. *J. Hydrol. Reg. Stud.* **2020**, *30*, 100710. [CrossRef]
40. Olivry, J.-C.; Bricquet, J.-P.; Thiébaux, J.-P.; Sigha-Nkamdjou, L. Transport de matière sur les grands fleuves des régions intertropicales: Les premiers résultats des mesures de flux particulaires sur le bassin du fleuve Congo. In *Sediment Budgets*; AISH: Porto-Alegre, Brazil, 1988; pp. 509–521.
41. Olivry, J.C.; Bricquet, J.P.; Laraque, A.; Guyot, J.L. Flux Liquides, Dissous et Particulaires de Deux Grands Bassins Intertropicaux: Le Congo à Brazzaville et Le Rio Madeira à Villabella. In *Grands Bassins Fluviaux Périatlantiques: Congo, Niger, Amazone*; Olivry, J.C., Boulegue, J., Eds.; IRD: Marseille, France, 1995; pp. 345–355.
42. Coynel, A.; Seyler, P.; Etcheber, H.; Meybeck, M.; Orange, D. Spatial and seasonal dynamics of total suspended sediment and organic carbon species in the Congo River. *Glob. Biogeochem. Cycles* **2005**, *19*, 1–17. [CrossRef]

43. Laraque, A.; Castellanos, B.; Steiger, J.; Lòpez, J.L.; Pandi, A.; Rodriguez, M.; Rosales, J.; Adèle, G.; Perez, J.; Lagane, C. A comparison of the suspended and dissolved matter dynamics of two large inter-tropical rivers draining into the Atlantic Ocean: The Congo and the Orinoco. *Hydrol. Process.* **2013**, *27*, 2153–2170. [CrossRef]
44. Wechsler, S.P. Uncertainties associated with digital elevation models for hydrologic applications: A review. *Hydrol. Earth Syst. Sci.* **2007**, *11*, 1481–1500. [CrossRef]
45. Nachtergaele, F.A.; van Velthuizen, H.B.; Batjes, N.C.; Dijkshoorn, K.C.; van Engelen, V.C.; Fischer, G.B.; Jones, A.D.; Montanarella, L.D.; Petri, M.A.; Prieler, S.B.; et al. The Harmonized World Soil Database Food and Agriculture Organization of the United Nations. In Proceedings of the World Congress of Soil Science, Soil Solutions for a Changing World, Brisbane, Australia, 1–6 August 2010; Published on DVD. pp. 34–37.
46. Huffman, G.J.; Bolvin, D.T.; Nelkin, E.J.; Wolff, D.B.; Adler, R.F.; Gu, G.; Hong, Y.; Bowman, K.P.; Stocker, E.F. The TRMM Multisatellite Precipitation Analysis (TMPA): Quasi-Global, Multiyear, Combined-Sensor Precipitation Estimates at Fine Scales. *J. Hydrometeorol.* **2007**, *8*, 38–55. [CrossRef]
47. Hartmann, J.; Moosdorf, N. The new global lithological map database GLiM: A representation of rock properties at the Earth surface. *Geochem. Geophys. Geosystems* **2012**, *13*, 1–37. [CrossRef]
48. Shekhar, S.; Xiong, H. Soil and Water Assessment Tool "SWAT". *Texas Water Resour. Inst.* **2008**, 1068. [CrossRef]
49. Zhou, P.; Huang, J.; Pontius, R.G.; Hong, H. New insight into the correlations between land use and water quality in a coastal watershed of China: Does point source pollution weaken it? *Sci. Total Environ.* **2016**, *543*, 591–600. [CrossRef] [PubMed]
50. Datok, P.; Fabre, C.; Sauvage, S.; N'kaya, G.M.; Paris, A.; Dos Santos, V.; Laraque, A.; Sánchez Pérez, J.-M. Investigating the role of the Cuvette Centrale in the hydrology of the Congo River Basin. In *Congo Basin Hydrology, Climate, and Biogeochemistry: A Foundation for the Future*; Geophysical Monograph Series; Alsdorf, D., Moukandi, G., Tshimanga, R., Eds.; John Wiley & Sons Inc.: Hoboken, NJ, USA, 2021. [CrossRef]
51. Gupta, H.V.; Kling, H.; Yilmaz, K.K.; Martinez, G.F. Decomposition of the mean squared error and NSE performance criteria: Implications for improving hydrological modelling. *J. Hydrol.* **2009**, *377*, 80–91. [CrossRef]
52. Williams, J.R. Sediment yield prediction with universal equation using runoff energy factor. In *Present and Prospective Technology for Predicting Sediment Yields and Sources, Proceedings of the Sediment-Yield Workshop, USDA Sedimentation Laboratory, Oxford, MI, USA, 17–18 January 1973*; U.S. Department of Agriculture, Agricultural Research Service: Washington, DC, USA, 1975; pp. 244–252.
53. Wischmeier, W.H.; Smith, D.D. *Predicting Rainfall-Erosion Losses: A Guide to Conservation Planning*; USDA Agriculture Handbook; Department of Agriculture, Science and Education Administration: Washington, DC, USA, 1978; p. 537.
54. Wischmeier, W.H.; Smith, D.D. *Predicting Rainfall-Erosion Losses from Croplands East of the Rocky Mountains*; USDA Agriculture Handbook; Department of Agriculture, Science and Education Administration: Washington, DC, USA, 1965; Volume 282, p. 47.
55. Vigiak, O.; Malagó, A.; Bouraoui, F.; Vanmaercke, M.; Poesen, J. Adapting SWAT hillslope erosion model to predict sediment concentrations and yields in large Basins. *Sci. Total Environ.* **2015**, *538*, 855–875. [CrossRef]
56. Jha, M.; Gassman, P.W.; Secchi, S.; Gu, R.; Arnold, J. Effect of watershed subdivision on swat flow, sediment, and nutrient predictions. *JAWRA* **2004**, *40*, 811–825. [CrossRef]
57. Borselli, L.; Cassi, P.; Sanchis, P. Soil Erodibility Assessment for Applications at Watershed Scale. In *Manual of Methods for Soil and Land Evaluation*; Science Publishers: Enfield, NH, USA, 2009. [CrossRef]
58. Borselli, L.; Torri, D.; Poesen, J.; Iaquinta, P. A robust algorithm for estimating soil erodibility in different climates. *Catena* **2012**, *97*, 85–94. [CrossRef]
59. Torri, D.; Poesen, J. Erodibilità. In *Metodi di Analisi Fisica del Suolo*; Pagliai, M., Ed.; Sezione VII; Ministero Delle Politiche Agricole e Forestali-Societa Italiana di Scienza del Suolo: Rome, Italy, 1997.
60. Torri, D.; Poesen, J.; Borselli, L. Corrigendum to "Predictability and uncertainty of the soil erodibility factor using a global dataset" [Catena 31 (1997) 1–22] and to "Erratum to Predictability and uncertainty of the soil erodibility factor using a global dataset" [Catena 32 (1998) 307–308]. *Catena* **2002**, *46*, 309–310. [CrossRef]
61. Shirazi, M.A.; Boersma, L.; Hart, J.W. A Unifying Quantitative Analysis of Soil Texture: Improvement of Precision and Extension of Scale. *Soil Sci. Soc. Am. J.* **1988**, *52*, 181–190. [CrossRef]
62. Sanchis, M.P.S.; Torri, D.; Borselli, L.; Poesen, J. Climate effects on soil erodibility. *Earth Surf. Process. Landf.* **2007**, *33*, 1082–1097. [CrossRef]
63. Engelen, V.; Verdoodt, A.; Dijkshoorn, J.A.; Van Ranst, E. *Soil and Terrain Database of Central Africa (DR of Congo, Burundi and Rwanda)*; Report 2006/07; ISRIC—World Soil Information: Wageningen, The Netherlands, 2006; Available online: http://www.isric.org (accessed on 13 May 2021).
64. Peel, M.C.; Finlayson, B.L.; McMahon, T.A. Updated world map of the Köppen-Geiger climate classification. *Hydrol. Earth Syst. Sci.* **2007**, *11*, 1633–1644. [CrossRef]
65. Bouillon, S.; Yambélé, A.; Spencer, R.G.M.; Gillikin, D.P.; Hernes, P.J.; Six, J.; Merckx, R.; Borges, A. Organic matter sources, fluxes and greenhouse gas exchange in the Oubangui River (Congo River basin). *Biogeosciences* **2012**, *9*, 2045–2062. [CrossRef]
66. Bouillon, S.; Yambélé, A.; Gillikin, D.P.; Teodoru, C.; Darchambeau, F.; Lambert, T.; Borges, A.V. Contrasting biogeochemical characteristics of the Oubangui River and tributaries (Congo River basin). *Sci. Rep.* **2014**, *4*, 5402. [CrossRef] [PubMed]
67. Laraque, A.; Mahé, G.; Orange, D.; Marieu, B. Spatiotemporal variations in hydrological regimes within Central Africa during the XXth century. *J. Hydrol.* **2001**, *245*, 104–117. [CrossRef]

68. Laraque, A.; Bellanger, M.; Adele, G.; Guebanda, S.; Gulemvuga, G.; Pandi, A.; Paturel, J.E.; Robert, A.; Tathy, J.P.; Yambele, A. Evolutions Récentes Des Débits Du Congo, de l'Oubangui et de La Sangha. *Geo. Eco. Trop.* **2013**, *37*, 93–100.
69. Vanmaercke, M.; Poesen, J.; Broeckx, J.; Nyssen, J. Sediment yield in Africa. *Earth Sci. Rev.* **2014**, *136*, 350–368. [CrossRef]
70. Moriasi, D.N.; Gitau, M.W.; Pai, N.; Daggupati, P. Hydrologic and Water Quality Models: Performance Measures and Evaluation Criteria. *Trans. ASABE* **2015**, *58*, 1763–1785. [CrossRef]
71. Adla, S.; Tripathi, S.; Disse, M. Can We Calibrate a Daily Time-Step Hydrological Model Using Monthly Time-Step Discharge Data? *Water* **2019**, *11*, 1750. [CrossRef]
72. Chishugi, J.B.; Alemaw, B.F. The Hydrology of the Congo River Basin: A GIS-Based Hydrological Water Balance Model. In *Proceedings of the World Environmental and Water Resources Congress*; Starett, S., Ed.; American Society of Civil Engineers (ASCE): Reston, VA, USA, 2009; pp. 1–16.
73. Tshimanga, R.M. Hydrological Uncertainty Analysis and Scenario-Based Streamflow Modelling for the Congo River Basin. Ph.D. Thesis, Rhodes University, Makhanda, South Africa, February 2012.
74. Tshimanga, R.M.; Hughes, D.A. Basin-scale performance of a semidistributed rainfall-runoff model for hydrological predictions and water resources assessment of large rivers: The Congo River. *Water Resour. Res.* **2014**, *50*, 1174–1188. [CrossRef]
75. Munzimi, Y.A.; Hansen, M.C.; Asante, K.O. Estimating daily streamflow in the Congo Basin using satellite-derived data and a semi-distributed hydrological model. *Hydrol. Sci. J.* **2019**, *64*, 1472–1487. [CrossRef]
76. Megnounif, A.; Terfous, A.; Ouillon, S. A graphical method to study suspended sediment dynamics during flood events in the Wadi Sebdou, NW Algeria (1973–2004). *J. Hydrol.* **2013**, *497*, 24–36. [CrossRef]
77. Laraque, A.; Olivry, J.C. Evolution de l'hydrologie Du Congo-Zaïre et de Ses Affluents Rive Droite et Dynamique Des Transports Solides et Dissous. *IAHS Publ.* **1996**, *238*, 271–288.
78. Laraque, A.; Maziezoltla, B. *Banque de Données Hydrologiques Des Affluents Congolais Du Fleuve Congo-Zaïre et Informations Physiographiques*; Programme PEGI/GBF, Volet Congo-UR22/DEC; ORSTOM—Laboratorie D'hydrologie: Montpellier, France, 1995; p. 250.
79. Aich, V.; Zimmermann, A.; Elsenbeer, H. Quantification and interpretation of suspended-sediment discharge hysteresis patterns: How much data do we need? *Catena* **2014**, *122*, 120–129. [CrossRef]
80. Malutta, S.; Kobiyama, M.; Chaffe, P.L.B.; Bonumá, N.B. Hysteresis analysis to quantify and qualify the sediment dynamics: State of the art. *Water Sci. Technol.* **2020**, *81*, 2471–2487. [CrossRef]
81. Nguimalet, C.-R.; Orange, D. Recent Hydrological Dynamics of Oubangui at Bangui (Central African Republic): Anthropogenic or Climatic Impacts? *Geo. Eco. Trop.* **2013**, *37*, 101–112.
82. Runge, J. The Congo River, Central Africa. *Large Rivers* **2008**, 293–309. [CrossRef]
83. Carr, A.B.; Trigg, M.A.; Tshimanga, R.M.; Borman, D.J.; Smith, M.W. Greater Water Surface Variability Revealed by New Congo River Field Data: Implications for Satellite Altimetry Measurements of Large Rivers. *Geophys. Res. Lett.* **2019**, *46*, 8093–8101. [CrossRef]
84. Marco, P.; Van Griensven, A. *Suitability of SWAT Model for Sediment Yields Modelling in the Eastern Africa*; Technical Paper; University of Dares Salam: Dares Salaam, Tanzania, 2011. [CrossRef]
85. Mayaux, P.; Bartholomé, E.; Massart, M.; Van Cutsem, C.; Cabral, A.; Nonguierma, A.; Diallo, O.; Pretorius, C.; Thompson, M.; Cherlet, M.; et al. A Land Cover Map of Africa. Carte de l'occupation Du Sol de l'Afrique. *EUR* **2003**, *20665*.
86. Ngongo, M.; Kasongo, E.; Muzinya, B.; Baert, G.; Van Ranst, E. Soil Resources in the Congo Basin: Their Properties and Constraints for Food Production. *Nutr. Food Prod. Congo Basin* **2014**, *c*, 214.
87. O'Loughlin, F.; Neal, J.; Schumann, G.; Beighley, E.; Bates, P. A LISFLOOD-FP hydraulic model of the middle reach of the Congo. *J. Hydrol.* **2020**, *580*, 124203. [CrossRef]
88. O'Loughlin, F.; Trigg, M.A.; Schumann, G.J.-P.; Bates, P.D. Hydraulic characterization of the middle reach of the Congo River. *Water Resour. Res.* **2013**, *49*, 5059–5070. [CrossRef]
89. Molliex, S.; Kettner, A.J.; Laurent, D.; Droz, L.; Marsset, T.; Laraque, A.; Rabineau, M.; N'Kaya, G.D.M. Simulating sediment supply from the Congo watershed over the last 155 ka. *Quat. Sci. Rev.* **2019**, *203*, 38–55. [CrossRef]
90. Garzanti, E.; Vermeesch, P.; Vezzoli, G.; Andò, S.; Botti, E.; Limonta, M.; Dinis, P.; Hahn, A.; Baudet, D.; De Grave, J.; et al. Congo River sand and the equatorial quartz factory. *Earth Sci. Rev.* **2019**, *197*, 102918. [CrossRef]
91. Laraque, A.; Pouyaud, B.; Rocchia, R.; Robin, R.; Chaffaut, I.; Moutsambote, J.M.; Maziezoula, B.; Censier, C.; Albouy, Y.; Elenga, H.; et al. Origin and function of a closed depression in equatorial humid zones: The lakeTele in north Congo. *J. Hydrol.* **1998**, *207*, 236–253. [CrossRef]
92. Haensler, A.; Jacob, D.; Kabat, P.; Ludwig, F. *Climate Change Scenarios for the Congo Basin*; Climate Service Centre Report No. 11; Climate Service Center: Hamburg, Germany, 2013; ISBN 2192–4058.
93. Filizola, N.; Guyot, J.L. Suspended sediment yields in the Amazon basin: An assessment using the Brazilian national data set. *Hydrol. Process.* **2009**, *23*, 3207–3215. [CrossRef]
94. Meade, R.H.; Dunne, T.; Richey, J.E.; Santos, U.D.M.; Salati, E. Storage and Remobilization of Suspended Sediment in the Lower Amazon River of Brazil. *Science* **1985**, *228*, 488–490. [CrossRef] [PubMed]
95. Richey, J.E.; Meade, R.H.; Salati, E.; Devol, A.H.; Nordin, C.F.; Dos Santos, U. Water Discharge and Suspended Sediment Concentrations in the Amazon River: 1982–1984. *Water Resour. Res.* **1986**, *22*, 756–764. [CrossRef]

96. Wei, X.; Sauvage, S.; Ouillon, S.; Le, T.P.Q.; Orange, D.; Herrmann, M.; Sanchez-Perez, J.-M. A modelling-based assessment of suspended sediment transport related to new damming in the Red River basin from 2000 to 2013. *Catena* **2021**, *197*, 104958. [CrossRef]
97. Hughes, D.A.; Tshimanga, R.M.; Tirivarombo, S.; Tanner, J. Simulating wetland impacts on stream flow in southern Africa using a monthly hydrological model. *Hydrol. Process.* **2013**, *28*, 1775–1786. [CrossRef]
98. Sun, X.; Bernard-Jannin, L.; Garneau, C.; Volk, M.; Arnold, J.G.; Srinivasan, R.; Sauvage, S.; Sánchez-Pérez, J.M. Improved simulation of river water and groundwater exchange in an alluvial plain using the SWAT model. *Hydrol. Process.* **2016**, *30*, 187–202. [CrossRef]
99. Sun, X.; Bernard-Jannin, L.; Grusson, Y.; Sauvage, S.; Arnold, J.; Srinivasan, R.; Pérez, J.M.S. Using SWAT-LUD Model to Estimate the Influence of Water Exchange and Shallow Aquifer Denitrification on Water and Nitrate Flux. *Water* **2018**, *10*, 528. [CrossRef]
100. Sok, T.; Oeurng, C.; Ich, I.; Sauvage, S.; Sánchez-Pérez, J.M. Assessment of Hydrology and Sediment Yield in the Mekong River Basin Using SWAT Model. *Water* **2020**, *12*, 3503. [CrossRef]